CORA Cork Open Research Archive
Cartlann Taighde Oscailte Chorcaí

Title	Binary mixtures of flufenamic acid and its chloro, difluoromethyl and fluoromethyl analogues; incorporation and distribution in flufenamic acid crystals
Authors	Bourke, Timothy;Chiarella, Renato A.;Moynihan, Humphrey A.
Publication date	2026-08-10
Original Citation	Bourke, T, Chiarella, R A & Moynihan, H A 2026, 'Binary mixtures of flufenamic acid and its chloro, difluoromethyl and fluoromethyl analogues; incorporation and distribution in flufenamic acid crystals', CrystEngComm, vol. 28, no. 31, pp. 4516-4527. https://doi.org/10.1039/d6ce00346j
Type of publication	Article (peer-reviewed)
Link to publisher's version	https://www.scopus.com/pages/publications/105043794282 - 10.1039/d6ce00346j
Rights	© 2026, The Author(s). Published by the Royal Society of Chemistry. This article is licensed under a Creative Commons Attribution 4.0 Unported Licence. You can use material from this article in other publications without requesting further permissions from the RSC, provided that the correct acknowledgement is given. - https://creativecommons.org/licenses/by/4.0/
Download date	2026-11-03 00:40:19
Item downloaded from	https://hdl.handle.net/10468/19092

UCC
University College Cork, Ireland
Coláiste na hOllscoile Corcaigh

Supplementary Information (SI) for CrystEngComm.
This journal is © The Royal Society of Chemistry 2026

Binary mixtures of flufenamic acid and its chloro, difluoromethyl and fluoromethyl analogues; incorporation and distribution in flufenamic acid crystals.

Timothy Bourke[a], Renato A. Chiarella[b], Humphrey A. Moynihan[a]*

[a] Analytical and Biological Chemistry Research Facility / School of Chemistry / Synthesis and Solid State Pharmaceutical Centre, University College Cork, College Road, Cork Y12 K8AF, Ireland.

[b] Pharmaceutical Development, Alkermes Inc., 900 Winter Street, Waltham, MA 02451, USA.

SUPPLEMENTARY INFORMATION

Table of Contents

Synthesis and Characterisation (p.4)

Infra-red spectroscopy methods (p.4)

Nuclear Magnetic Resonance spectroscopy methods (p.4)

Mass spectrometry method (p.4)

Fig. S1 IR spectrum of **ClFA**. (p.4)

Fig. S2. Aromatic region of the ^{1}H NMR spectrum of **ClFA**. (p.5)

Fig. S3. Full ^{13}C NMR spectrum of **ClFA.** (p.5)

Fig. S4. Aromatic region of the ^{13}C NMR spectrum of **ClFA**. (p.6)

Fig. S5. IR spectrum of **HF_2FA**. (p.6)

Fig. S6. Aromatic region of the ^{1}H NMR spectrum of **HF_2FA**. (p.7)

Fig. S7. Full ^{13}C NMR spectrum of **HF_2FA**. (p.7)

Fig. S8. Aromatic region of the ^{13}C NMR spectrum of **HF_2FA**. (p.8)

Fig. S9. A portion of the aromatic region of the ^{13}C NMR spectrum of **HF_2FA**, illustrating the large splitting of the C^1 carbon peak due to coupling with two geminal fluorine atoms. (p.8)

Fig. S10. Aromatic region of the DEPT 90 NMR spectrum of **HF_2FA**. (p.9)

Fig. S11. Aromatic region of the DEPT 135 NMR spectrum of **HF_2FA**. (p.9)

Fig. S12. IR spectrum of **H_2FFA**. (p.10)

Fig. S13. Full ^{1}H NMR spectrum of **H_2FFA** showing the position of the C^1H_2F doublet signal outside the aromatic region. (p.10)

Fig. S14. Aromatic region of the ^{1}H NMR spectrum of **H_2FFA**. (p.11)

Fig. S15. Full ^{13}C NMR spectrum of **H_2FFA** showing the position of one quaternary carbon signal as well as the C^1H_2F doublet signal outside the aromatic region. (p.11)

Fig. S16. Aromatic region of the ^{13}C NMR spectrum of **H_2FFA**. (p.12)

Fig. S17. Aromatic region of the DEPT 90 NMR spectrum of **H_2FFA**. (p.12)

Fig. S18. Full DEPT 135 NMR spectrum of **H_2FFA**, with labelled peaks. (p.13)

Fig. S19. Aromatic region of the DEPT 135 NMR spectrum of **H_2FFA**.(p.13)

HPLC (p.14)

Fig. S20. Linear regression curve fitted to data points for standard solution of commercial **FFA** and the equation of that curve. (p.14)

Table S1 Regression statistics for the commercial **FFA** calibration curve, including *r* values. (p.14)

Table S2. Regression coefficient statistics for the commercial **FFA** calibration curve. (p.15)

Fig. S21. Calibration Curve for standard solutions of **ClFA** with linear regression curve equation. (p.15)

Table S3. Residual Statistics for **ClFA** Calibration Curve. (p.15)

Table S4. Residual Coefficients Statistics for **ClFA** calibration curve. (p.16)

Fig. S22. Calibration curve for **HF_2FA** with linear regression curve equation. (p.16)

Table S5. Residual Statistics for **HF_2FA** calibration curve. (p.16)

Table S6. Residual Coefficients Statistics for **HF_2FA** Calibration Curve. (p.17)

Fig. S23. Calibration curve for **H_2FFA** with linear regression curve equation. (p.17)

Table S7. Residual Statistics for **H_2FFA** Calibration Curve. (p.17)

Table S8. Residual Coefficients Statistics for **H_2FFA** Calibration Curve. (p.18)

Fig. S24. HPLC trace of a solution of **FFA** (right, 2.202 min) in acetonitrile containing approx. 2 mol% **ClFA** (left, 1.888 min). (p.18)

Fig. S25. HPLC trace of a solution of **FFA** (right, 2.209 min) in acetonitrile containing approx. 2 mol% **H_2FFA** (left, 1.311 min). (p.19)

Fig. S26 HPLC trace of a solution of **FFA** (right, 2.207 min) in acetonitrile containing approx. 2 mol% **HF_2FA** (left, 1.138 min). (p.19)

PXRD (p.20)

Fig. S27. Measured PXRD pattern of **FFA** recrystallised from EtOH (top) *vs.* literature patterns for Form III and Form I (bottom). (p.20)

Fig. S28. Top: Measured PXRD pattern of synthesised **ClFA**, bottom: literature patterns of **ClFA** Form I, Form II, and Form III. (p.21)

Crystallisations / Partial Dissolutions (p.22)

Fig. S29. Example of **FFA** crystals grown by the slow evaporation from methanol solution of FFA. (p.22)

Fig. S30. Surface area distributions for a sample of 20 **FFA** crystals, grown from MeOH solutions containing 2% **HF_2FA**, for the initial sample and for the sample after each of a series of four partial dissolutions. (p.22)

DSC (p.23)

Fig. S31. Top to bottom, DSC curves of **FFA** crystallised with 10 % **ClFA**, collected at heating rates of 1, 10, and 50 °C min^{-1} respectively. **Fig S32**. Top to bottom, DSC curves of **FFA** crystallised with 10%, 20%, 30% and 40% **ClFA**, respectively, collected at a heating rate of 1 min^{-1}. The inset in the top right shows the emergence of the higher melting endotherm. (p.23)

Fig. S32. Top to bottom, DSC curves of **FFA** crystallised with 10%, 20%, 30% and 40% **ClFA**, respectively, collected at a heating rate of 1 min^{-1}. The inset in the top right shows the emergence of the higher melting endotherm. (p.23)

Fig. S33. Bottom to top, DSC curves of **FFA** crystallised with 24%, 26%, 28% and 30% **ClFA**, respectively, collected at a heating rate of 1 °C min^{-1}. The insert on bottom right shows the emergence of the higher melting endotherm. (p.23)

Fig. S34. Top to bottom, DSC curves of **FFA** crystallised with 60%,70%, 80%, 90% **ClFA**, respectively, collected at a heating rate of 1 °C min^{-1}. (p.24)

Fig. S35. Bottom to top, DSC curves of **FFA** crystallised with increasing levels of **ClFA**, from 2% to 30%, collected at a heating rates of 1 °C min^{-1}. The insert on the bottom right is an expansion of the region enclosed in dashed lines. (p.25)

Fig. S36. DSC curves of **FFA** containing, bottom to top 0%, 2%, 3%, 4%, 5% and 100% **HF_2FA**, collected at a heating rate of 10 °C min^{-1}. (p.25)

Fig. S37. DSC curves of **FFA** containing, bottom to top, 0%, 2%, 3%, 4%, 5 % and 100% **H_2FFA**, collected at a heating rate of 10 °C min^{-1}. (p.26)

Fig. S38. Plot of **ClFA** level *vs* dissolution midpoint of a sample of 10 crystals of FFA grown from solution containing 2% **ClFA**. (p.26)

Fig. S39. Plot of **ClFA** level *vs* dissolution midpoint of a large single crystal of **FFA** grown from solution containing 2% **ClFA**. (p.27)

Fig. S40. Plot of α_2 value *vs.* dissolution midpoint a sample of 14 crystals or **FFA**, and also of a large single crystal of **FFA**, grown from solutions containing 2% **ClFA**. (p.27)

Fig. S41. Plot of **HF_2FA** level *vs* dissolution midpoint of three separate samples of crystals of **FFA** grown from solutions containing 2% **HF_2FA**. (p.28)

Synthesis and Characterisation

Infra-red spectra were recorded on a Perkin Elmer Spectrum 100 FT-IR Spectrometer using thin films between sodium chloride discs following evaporation of a solution of a small amount of the solid sample in a volatile solvent.

Nuclear Magnetic Resonance spectra were recorded, for ^{1}H NMR, at 300 MHz, and for ^{13}C NMR at 75.5 MHz, on a Bruker AVANCE 300 NMR spectrometer.

Mass spectrometry: Nominal mass spectra were recorded on a Waters Quattro Micro Triple Quadrupole Spectrometer (QAA1202) in ESI mode using 50% acetonitrile / water containing 0.1% formic acid as an eluent. High resolution mass spectra (HRMS) were recorded on a Waters LCT Premier Time of Flight spectrometer (KD160) or a Waters Vion IMS Mass Spectrometer (SAA0 55K) in ESI mode using 50% acetonitrile / water containing 0.1% formic acid as an eluent. Mass spectrometry samples were prepared in acetonitrile.

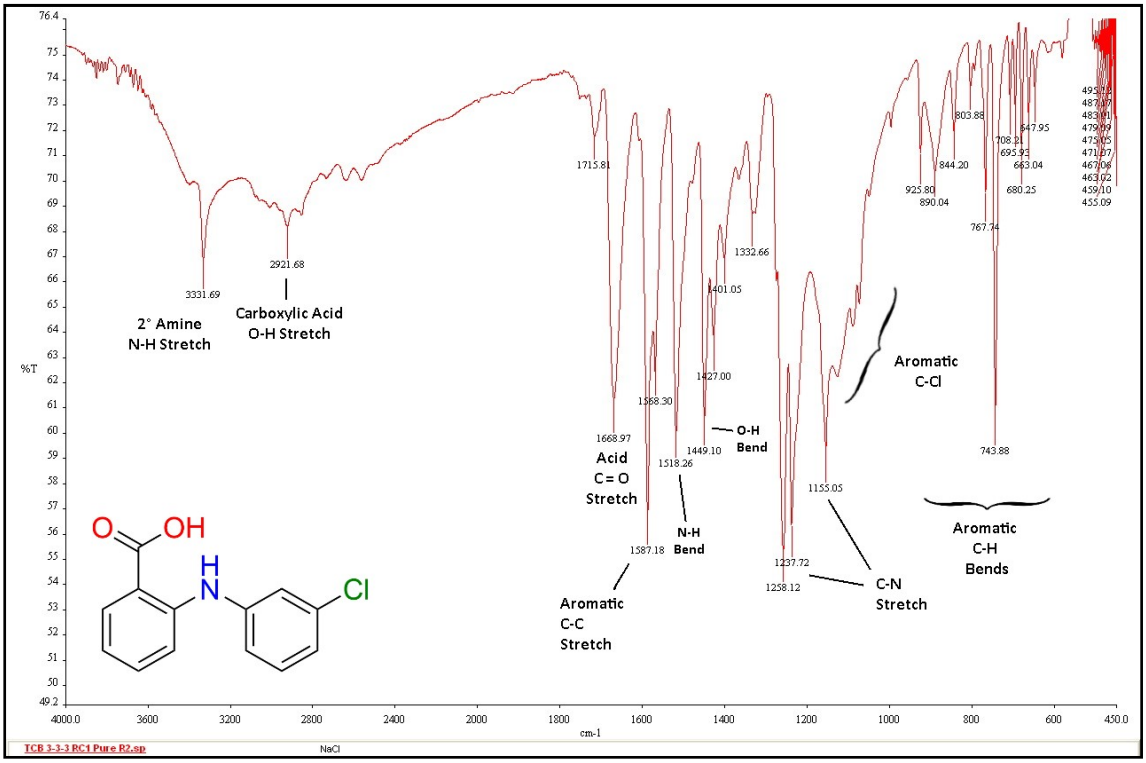


Fig. S1 IR spectrum of **ClFA**.

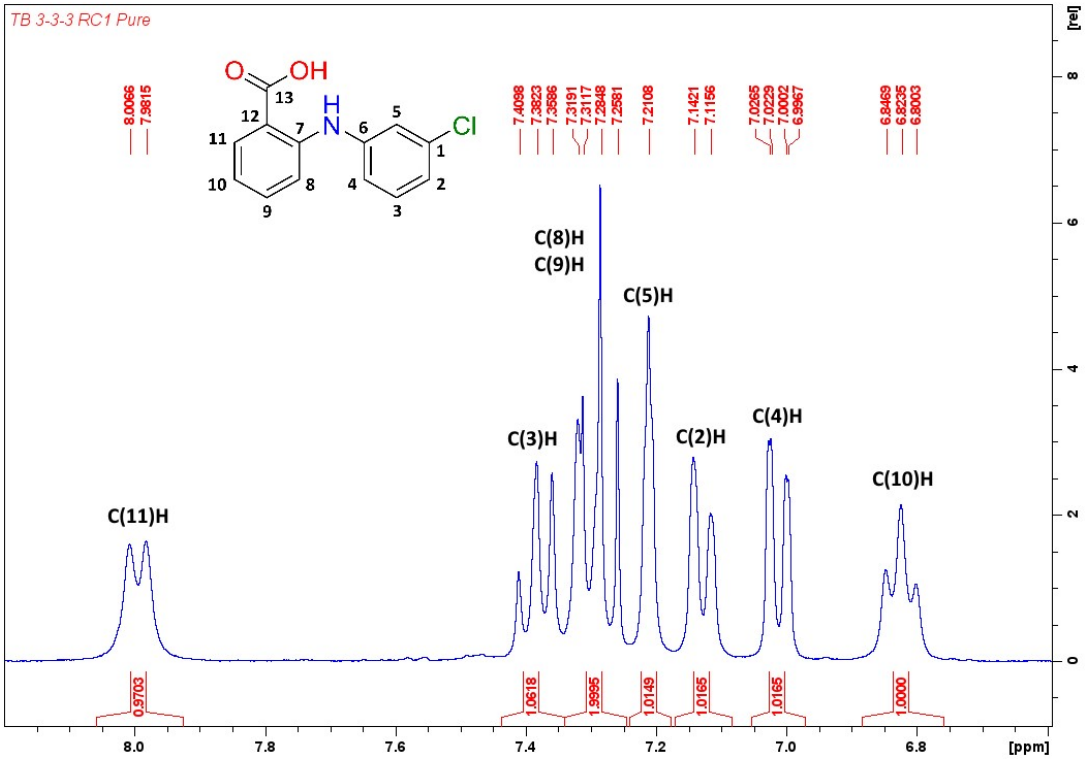


Fig. S2. Aromatic region of the ^{1}H NMR spectrum of **ClFA**.

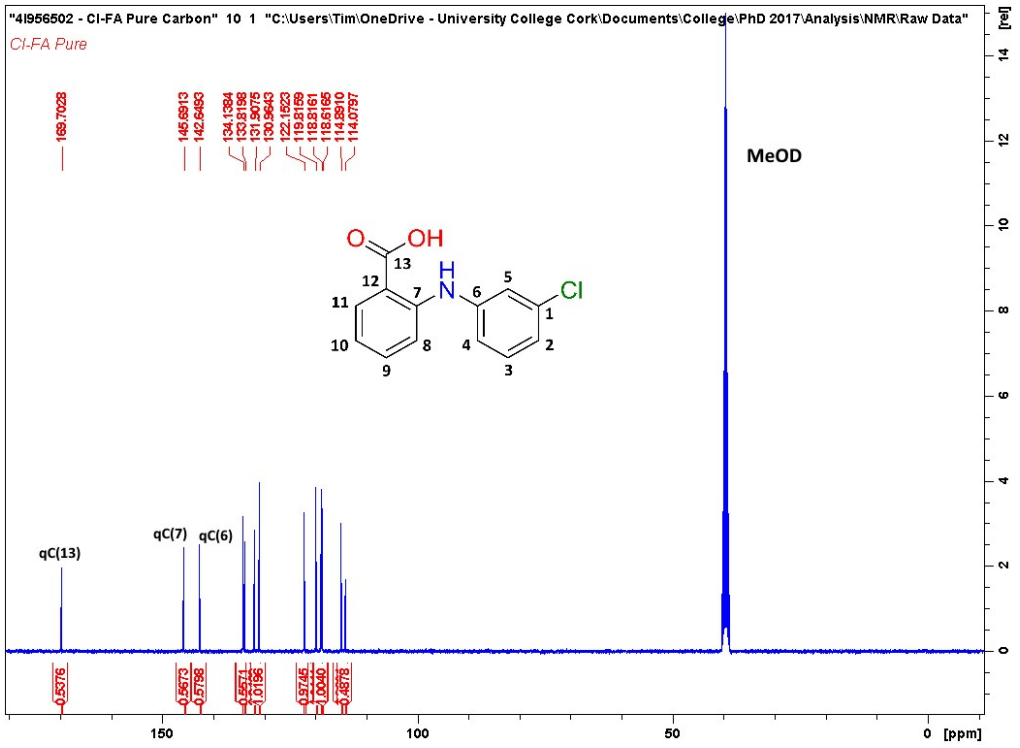


Fig. S3. Full ^{13}C NMR spectrum of **ClFA**.

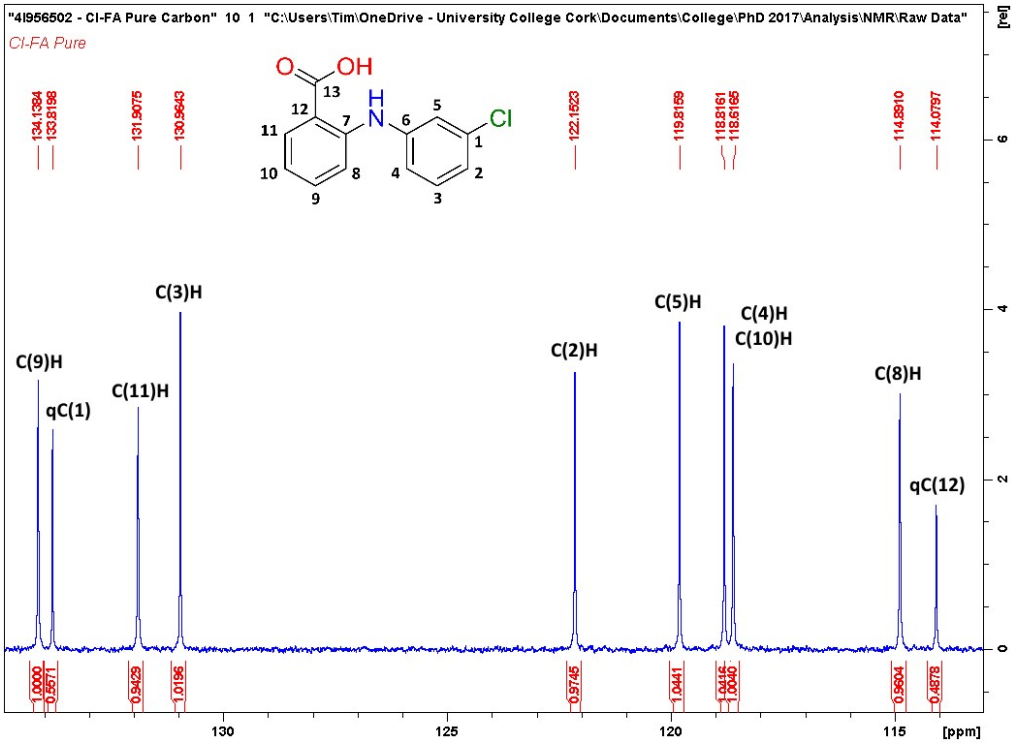


Fig. S4. Aromatic region of the ^{13}C NMR spectrum of **ClFA**.

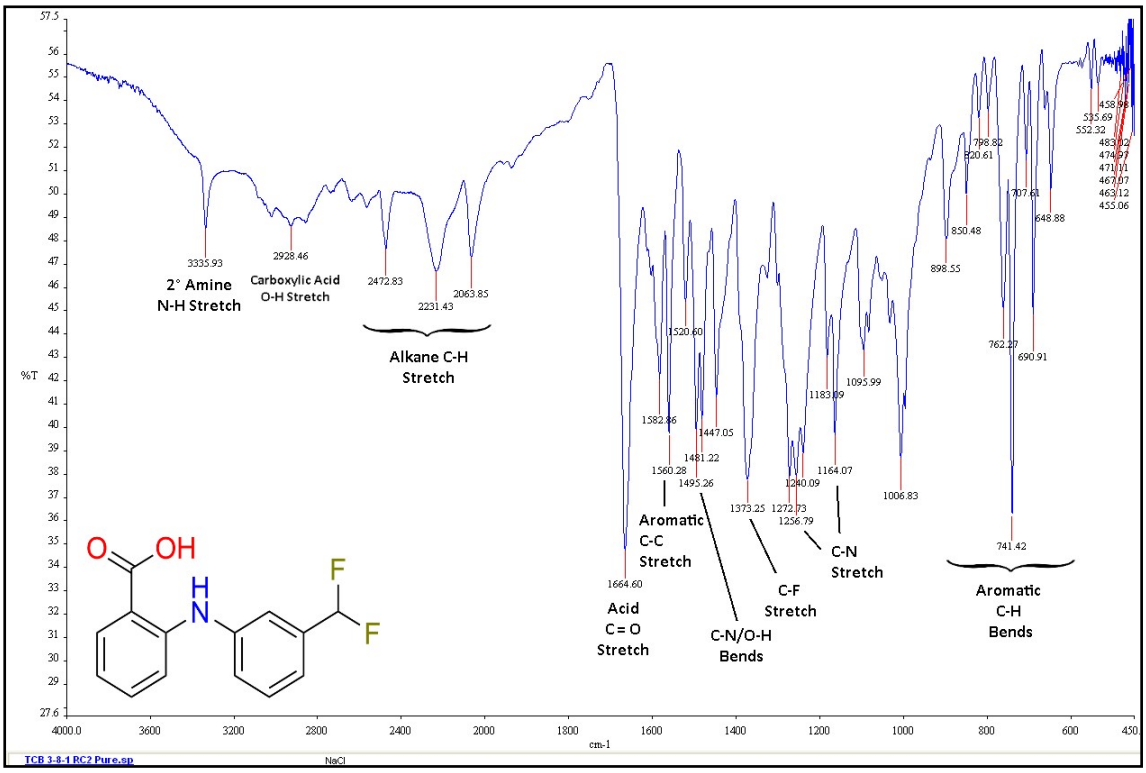


Fig. S5. IR spectrum of **HF_2FA**.

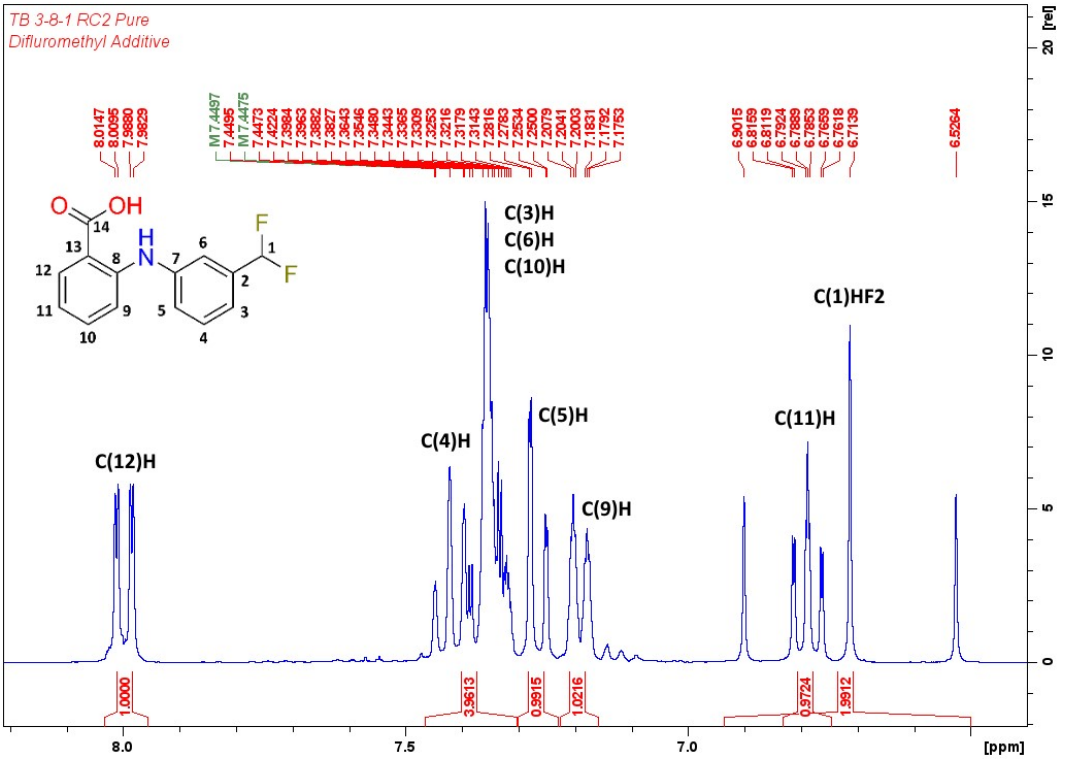


Fig. S6. Aromatic region of the ^{1}H NMR spectrum of **HF_2FA**.

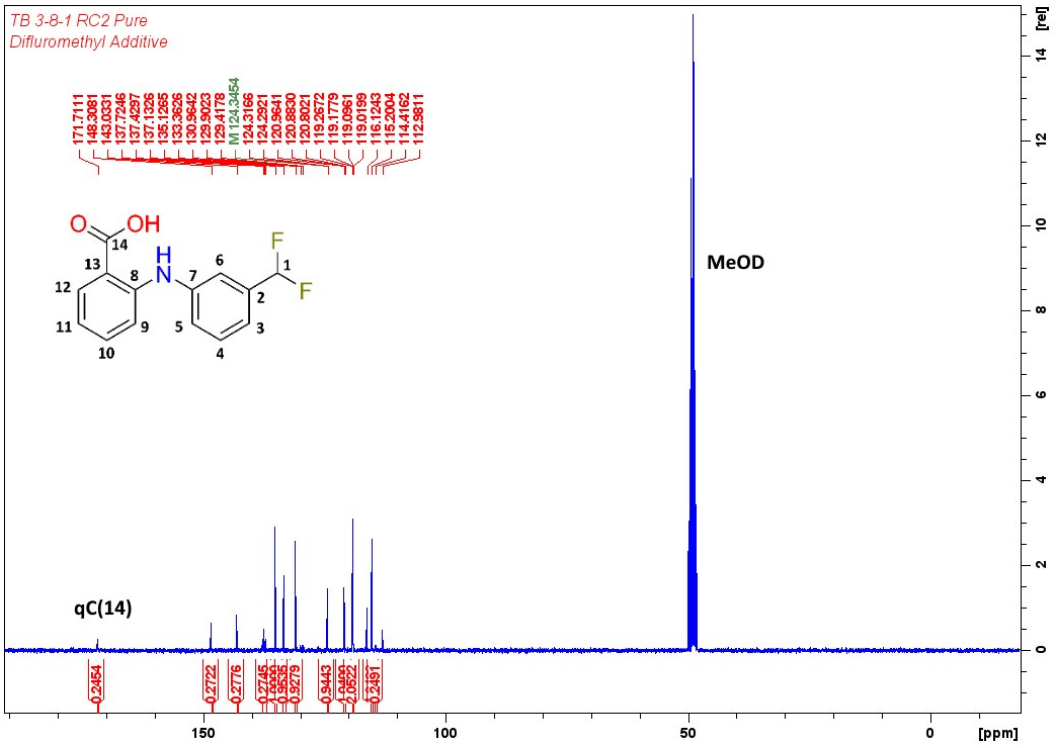


Fig. S7. Full ^{13}C NMR spectrum of **HF_2FA**.

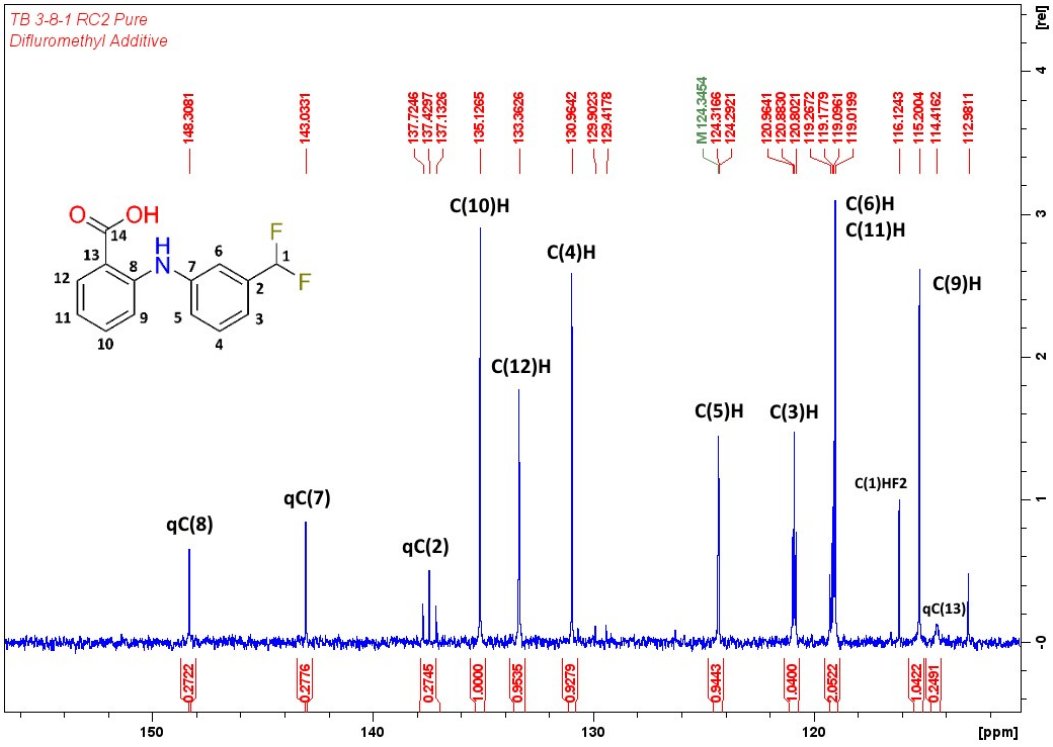


Fig. S8. Aromatic region of the ^{13}C NMR spectrum of **HF_2FA**.

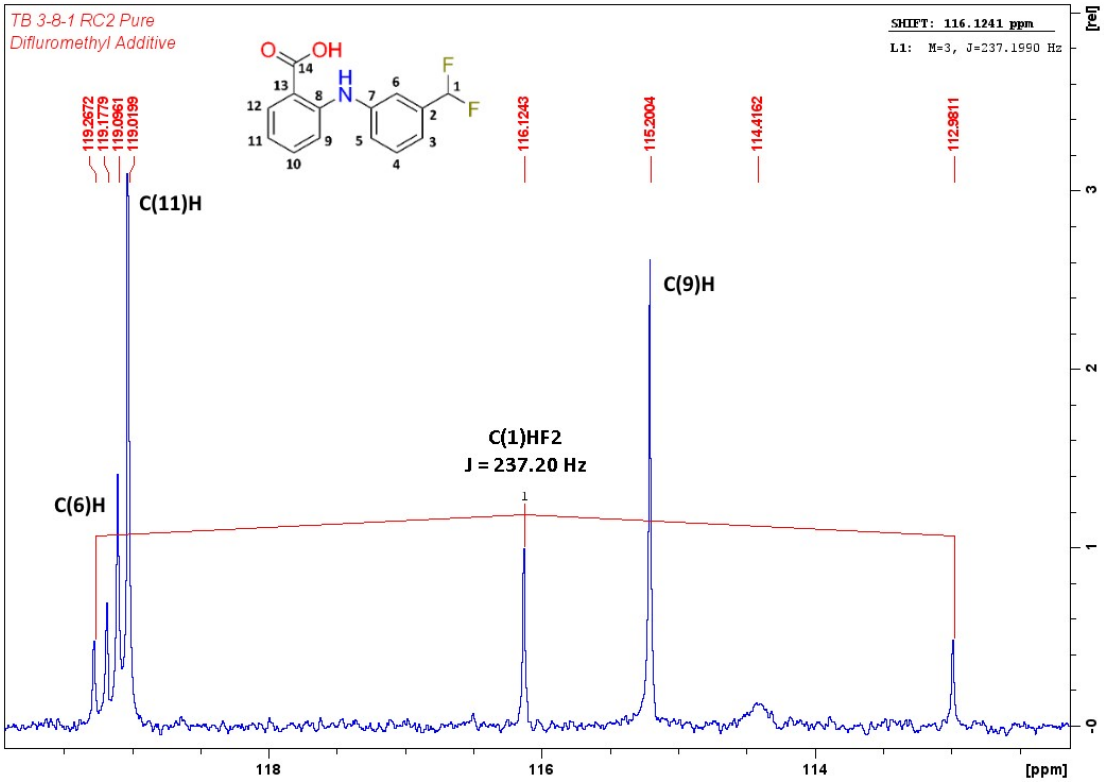


Fig. S9. A portion of the aromatic region of the ^{13}C NMR spectrum of **HF_2FA**, illustrating the large splitting of the C^1 carbon peak due to coupling with two geminal fluorine atoms.

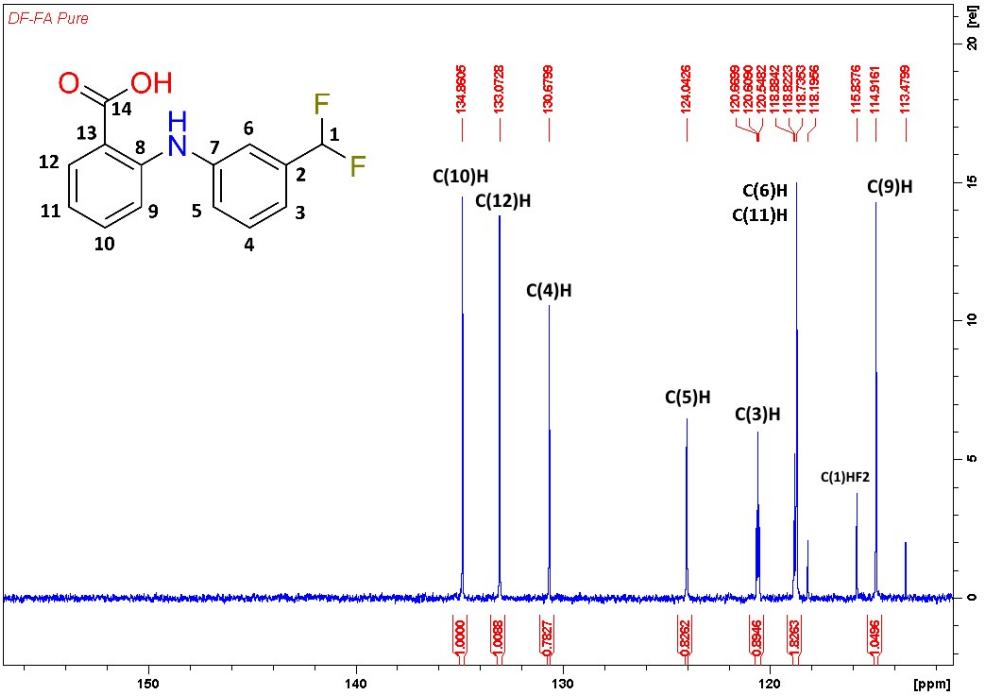


Fig. S10. Aromatic region of the DEPT 90 NMR spectrum of **HF_2FA**.

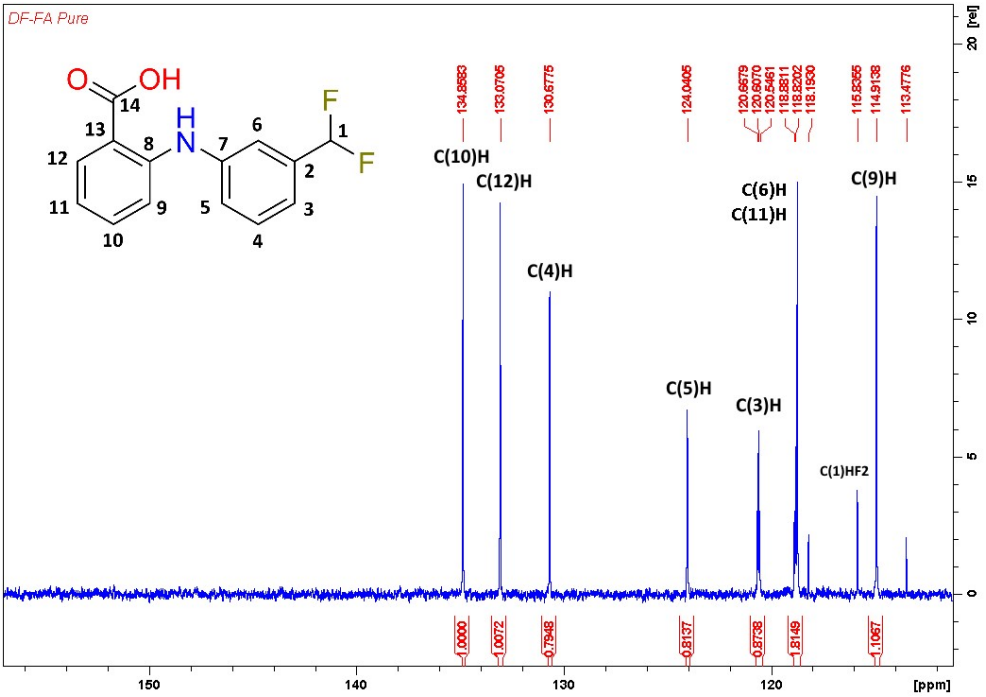


Fig. S11. Aromatic region of the DEPT 135 NMR spectrum of **HF_2FA**.

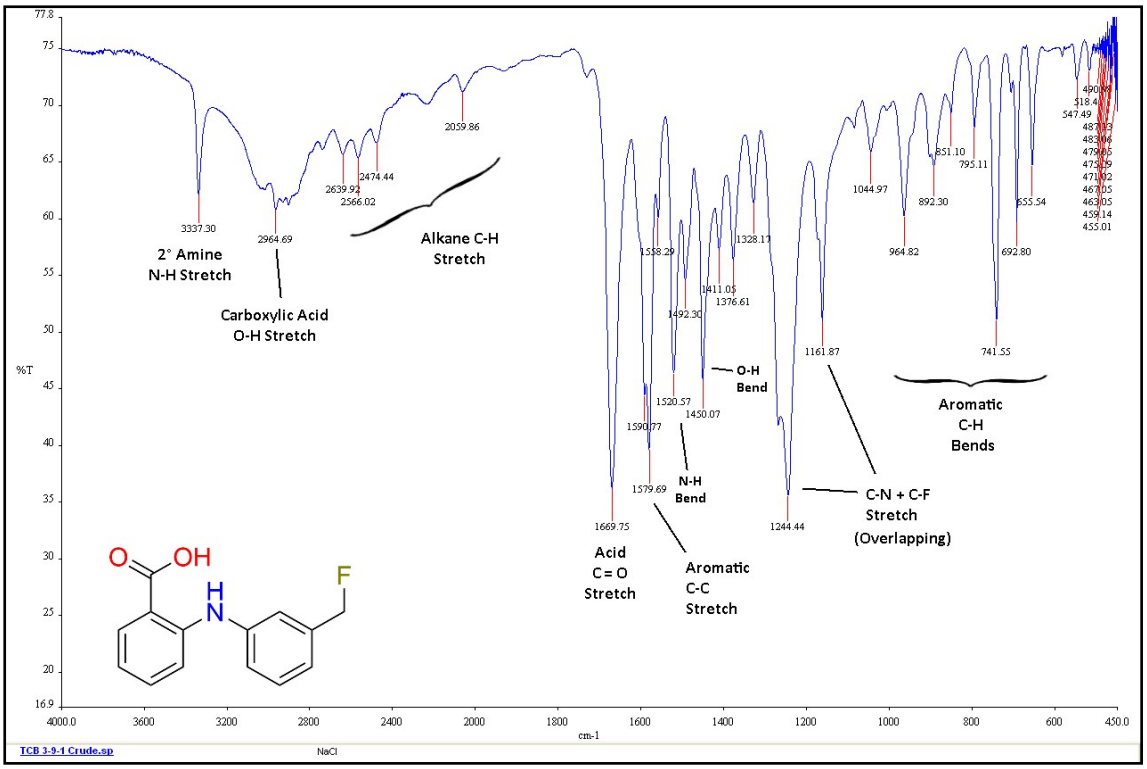


Fig. S12. IR spectrum of **H_2FFA**.

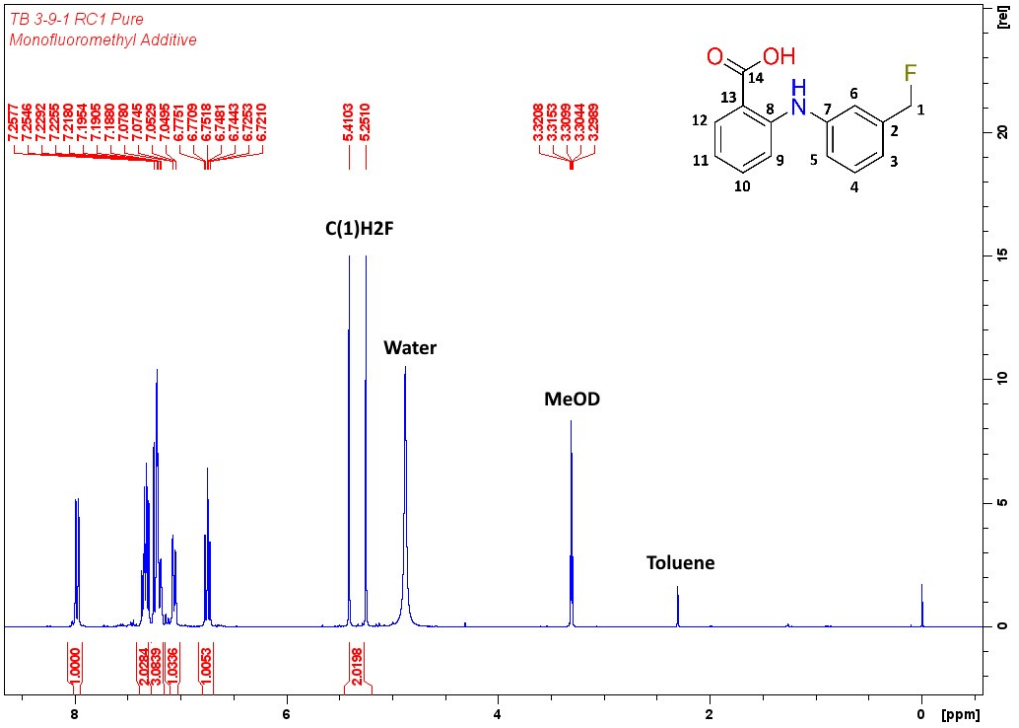


Fig. S13. Full ^{1}H NMR spectrum of **H_2FFA** showing the position of the C^{1}H$_2$F doublet signal outside the aromatic region.

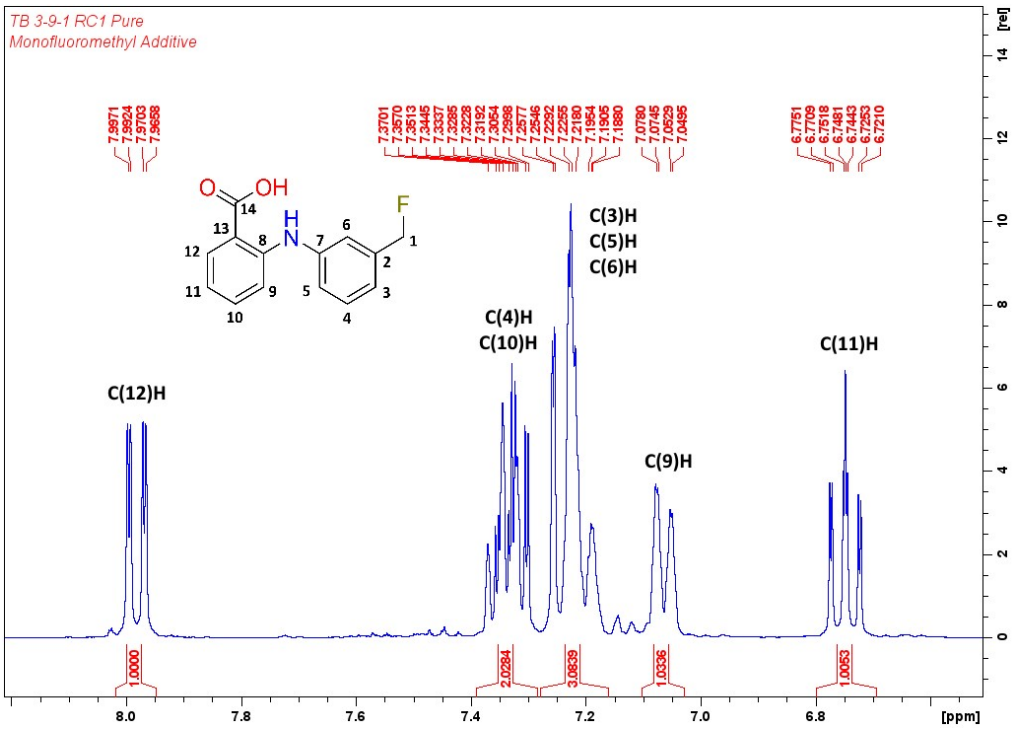


Fig. S14. Aromatic region of the ^{1}H NMR spectrum of **H_2FFA**.

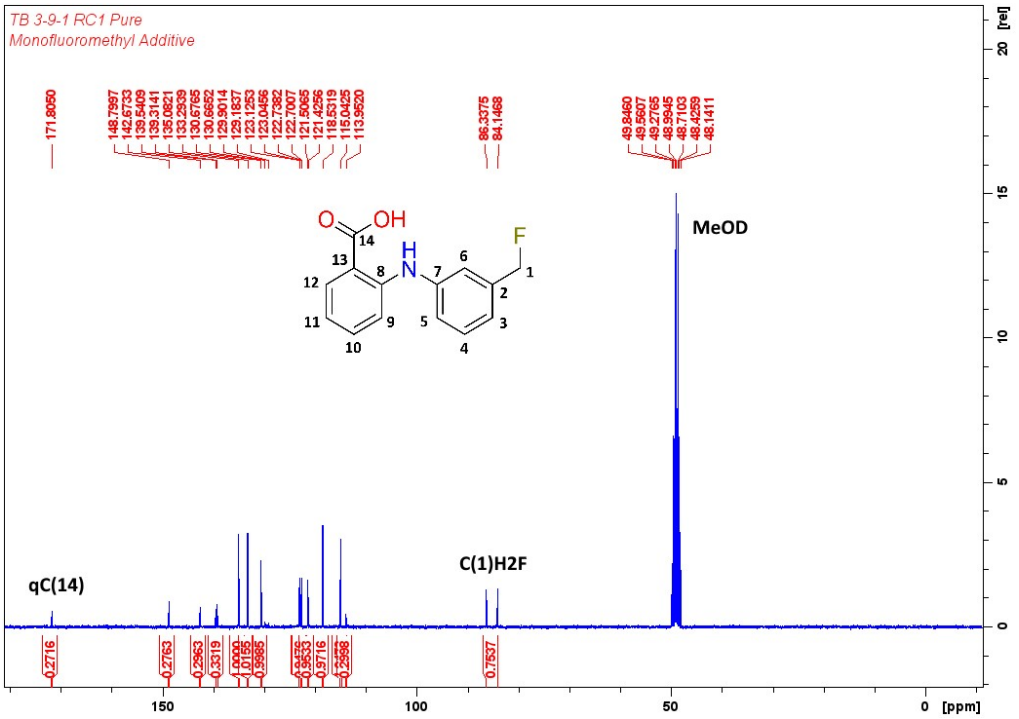


Fig. S15. Full ^{13}C NMR spectrum of **H_2FFA** showing the position of one quaternary carbon signal as well as the C^{1}H$_2$F doublet signal outside the aromatic region.

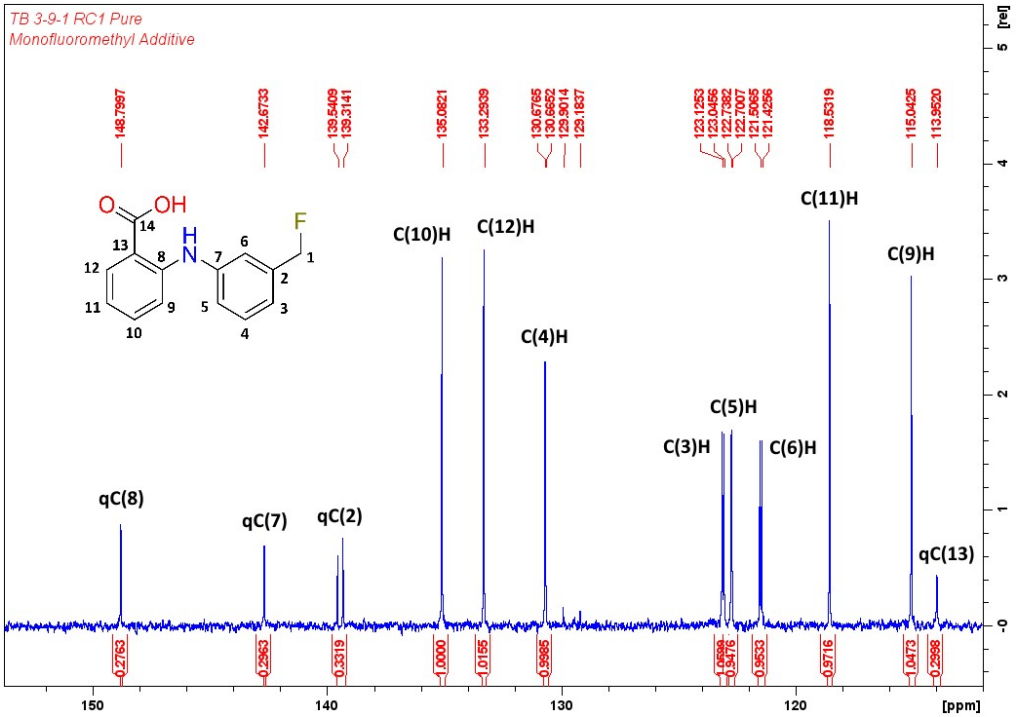


Fig. S16. Aromatic region of the ^{13}C NMR spectrum of **H_2FFA**.

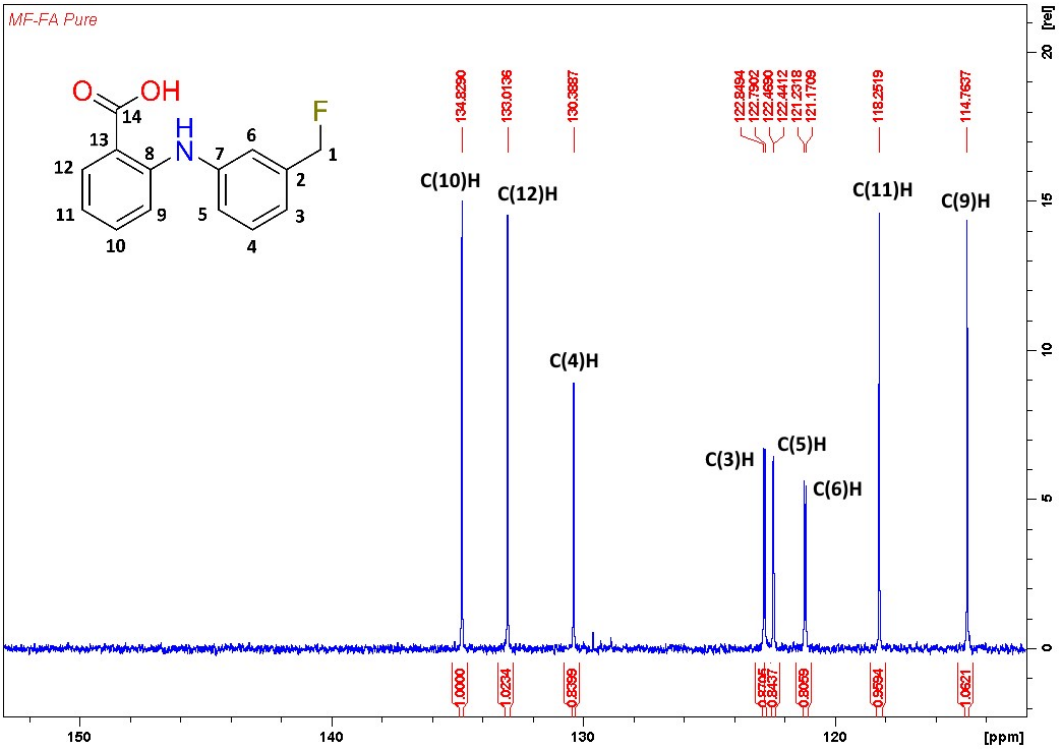


Fig. S17. Aromatic region of the DEPT 90 NMR spectrum of **H_2FFA**.

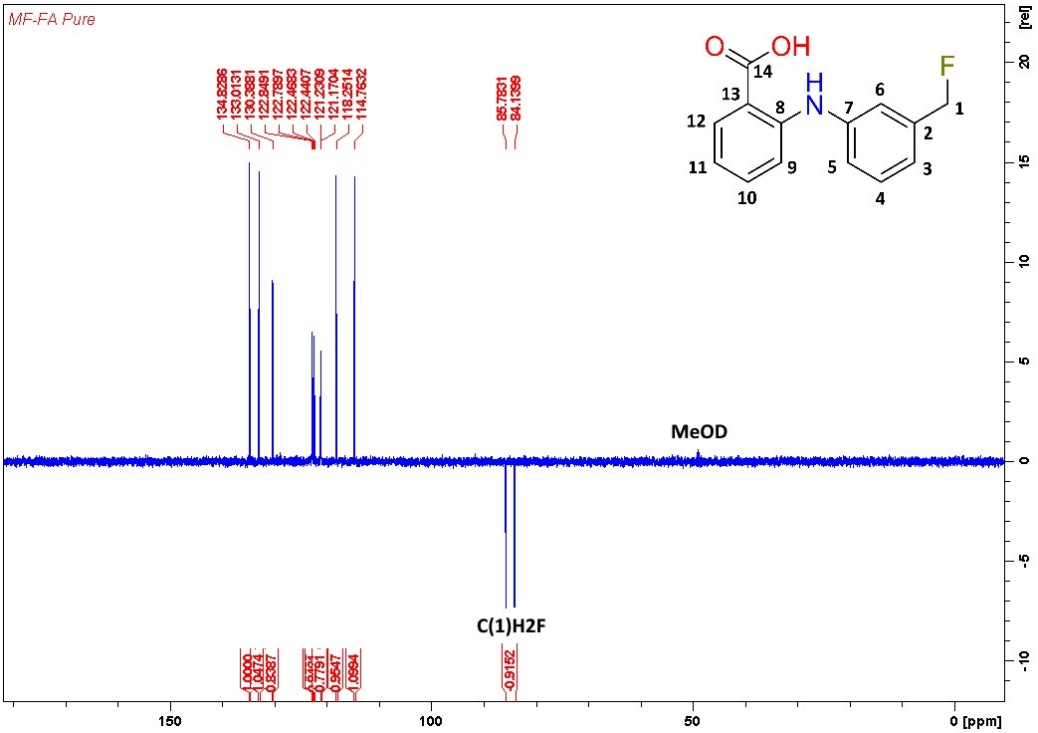


Fig. S18. Full DEPT 135 NMR spectrum of **H_2FFA**, with labelled peaks.

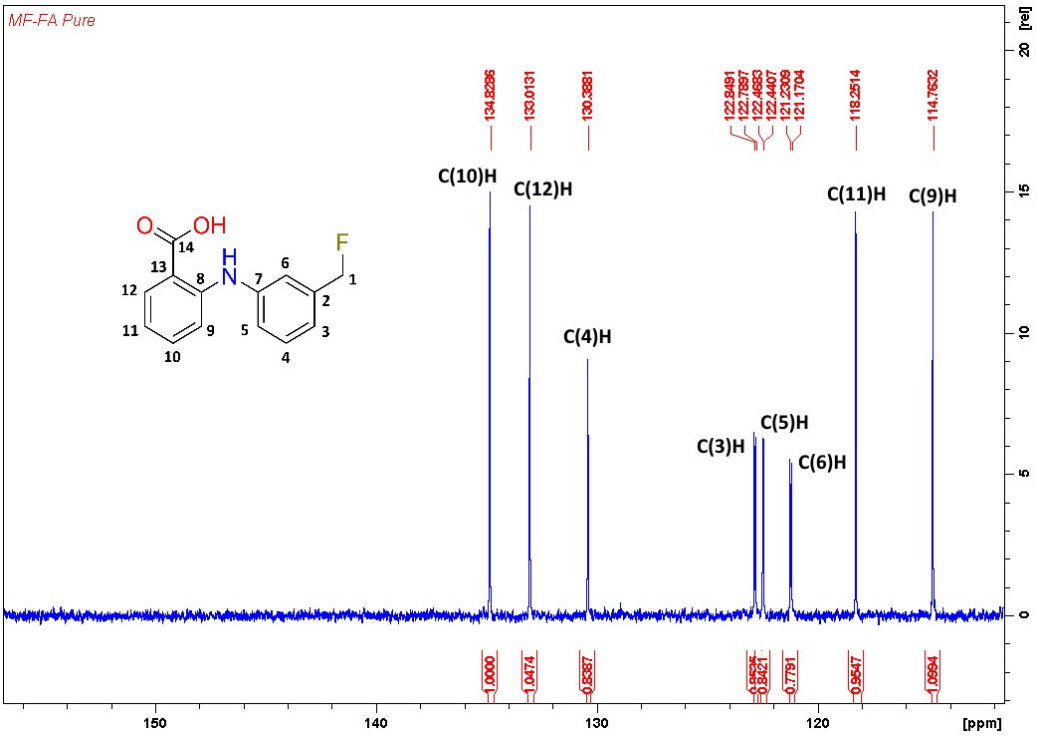


Fig. S19. Aromatic region of the DEPT 135 NMR spectrum of **H_2FFA**.

HPLC

Calibration curves

Four to seven standard solutions were prepared for each calibration curve. Standard solutions were produced by dissolving an appropriate mass of the material of interest in 100 mL of MeCN with thorough mixing, so that the concentrations of each standard fell between 0.25 and 2.20 mg mL^{-1}. Three aliquots were removed from each standard for analysis by HPLC. Each aliquot was analysed in triplicate by HPLC. The resulting calibration curves and statistics are shown in Figs. S20 to S23 and Tables S1 to S8 below. Examples of HPLC traces of solution of **FFA** containing quantities of either **ClFA**, **HF_2FA** or **H_2FFA** are shown in Figs. S24 to S26 below.

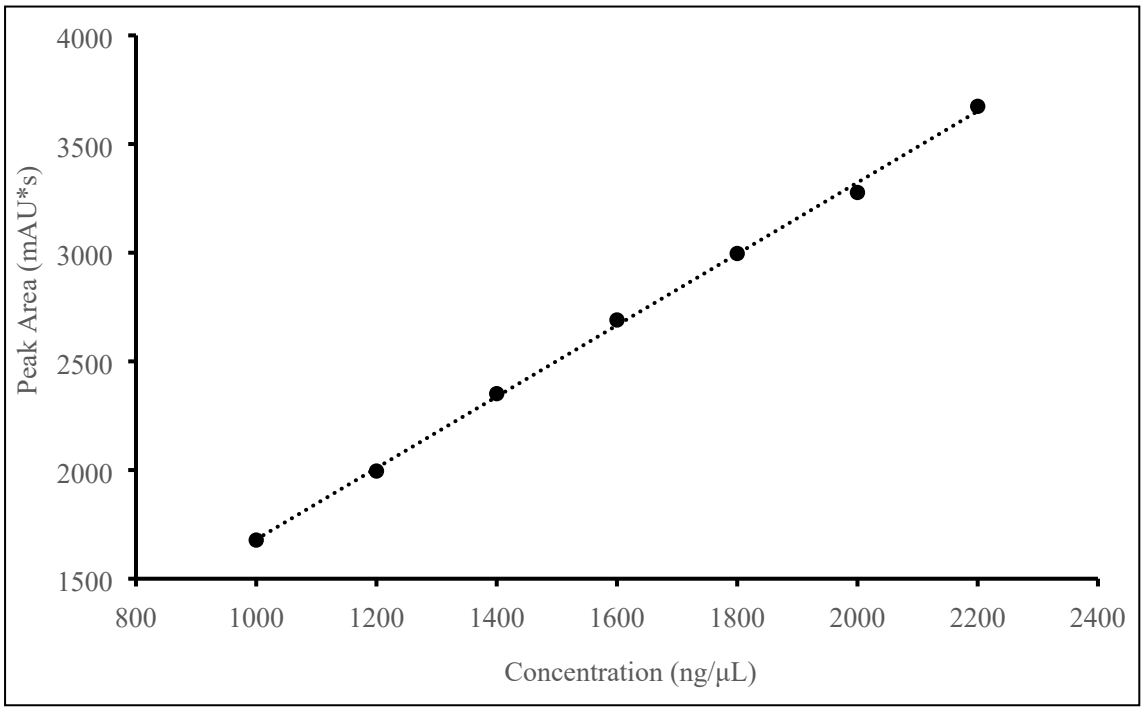


Fig. S20. Linear regression curve fitted to data points for standard solution of commercial **FFA** and the equation of that curve.

Table S1 Regression statistics for the commercial **FFA** calibration curve, including *r* values.

Multiple R	0.9994083
R Square	0.9988169
Adjusted R Square	0.9985802
Standard Error	26.7487195
Observations	7

Table S2. Regression coefficient statistics for the commercial **FFA** calibration curve.

	Coefficients	Standard Error	t Stat	P-value	Lower 95.0%	Upper 95.0%
Intercept	38.661	41.685	0.927	0.396	-68.494	145.81
Concentration (ng μL^{-1})	1.642	0.025	64.970	1.64E-08	1.577	1.707

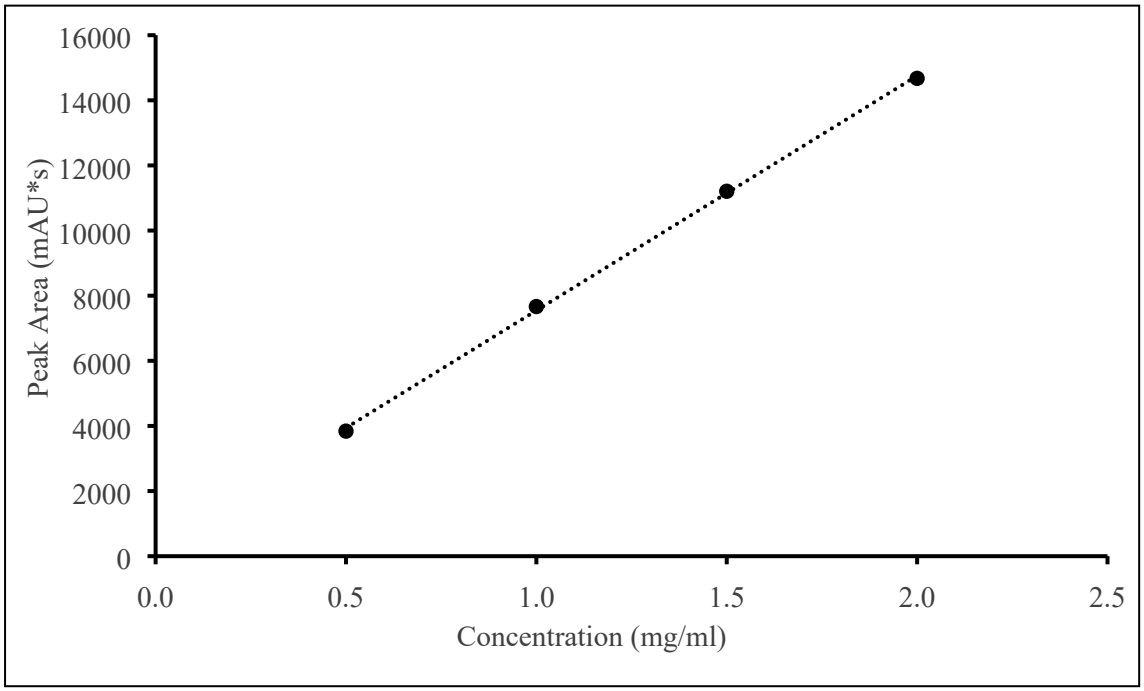


Fig. S21. Calibration Curve for standard solutions of **ClFA** with linear regression curve equation.

Table S3. Residual Statistics for **ClFA** Calibration Curve.

Multiple R	0.9997352
R Square	0.9994705
Adjusted R Square	0.9992057
Standard Error	131.1707562
Observations	4

Table S4. Residual Coefficients Statistics for **ClFA** calibration curve.

	Coefficients	Standard Error	t Stat	P-value	Lower 95.0%	Upper 95.0%
Intercept	337.065	160.651	2.098	0.171	-354.159	1028.289
Concentration (mg/mL)	7208.245	117.323	61.439	2.648E-04	6703.446	7713.044

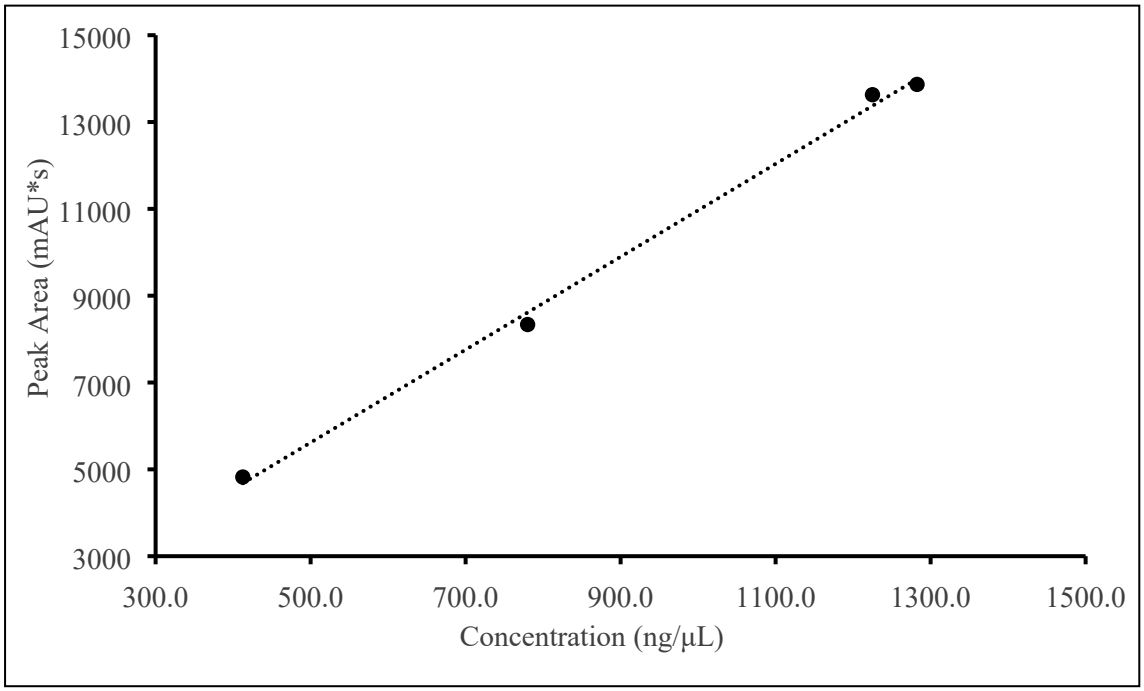


Fig. S22. Calibration curve for **HF_2FA** with linear regression curve equation.

Table S5. Residual Statistics for **HF_2FA** calibration curve.

Multiple R	0.9984595
R Square	0.9969214
Adjusted R Square	0.9953820
Standard Error	297.7301230
Observations	4

Table S6. Residual Coefficients Statistics for **HF_2FA** Calibration Curve.

	Coefficients	Standard Error	t Stat	P-value	Lower 95.0%	Upper 95.0%
Intercept	266.827	416.415	0.641	0.587	-1524.863	2058.517
Concentration (ng/μL)	10.699	0.420	25.449	0.002	8.890	12.508

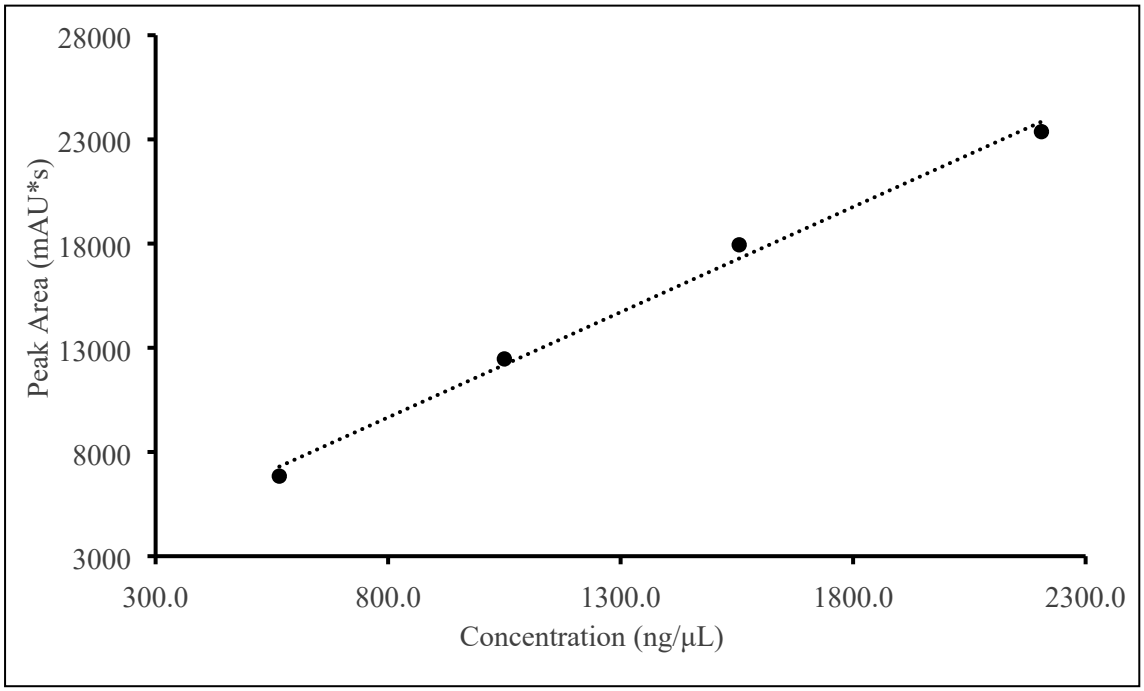


Fig. S23. Calibration curve for **H_2FFA** with linear regression curve equation.

Table S7. Residual Statistics for **H_2FFA** Calibration Curve.

Multiple R	0.9968719
R Square	0.9937536
Adjusted R Square	0.9906304
Standard Error	688.1365401
Observations	4

Table S8. Residual Coefficients Statistics for **H_2FFA** Calibration Curve.

	Coefficients	Standard Error	t Stat	P-value	Lower 95.0%	Upper 95.0%
Intercept	1582.955	835.034	1.896	0.198	-2009.905	5175.814
Concentration (ng/µL)	10.098	0.566	17.838	0.003	7.662	12.534

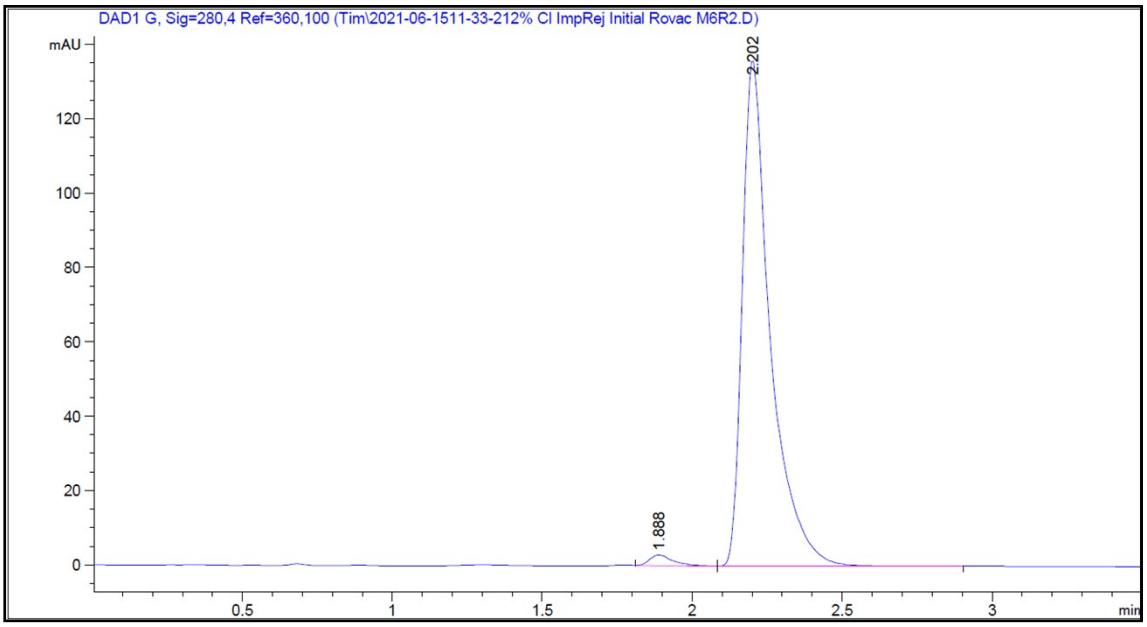


Fig. S24. HPLC trace of a solution of **FFA** (right, 2.202 min) in acetonitrile containing approx. 2 mol% **ClFA** (left, 1.888 min).

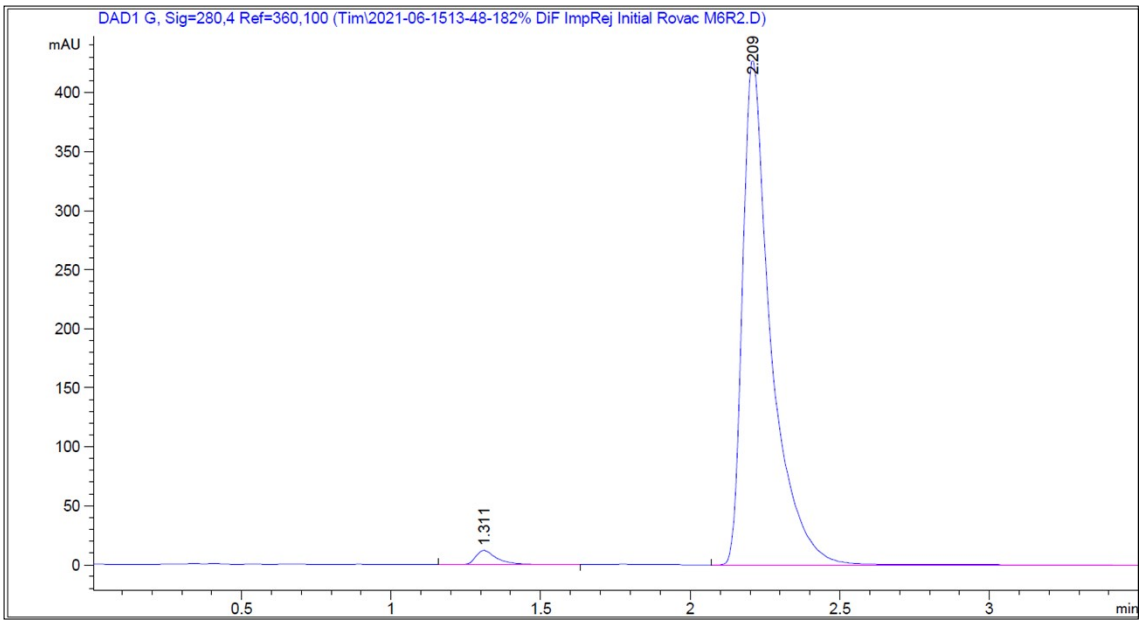


Fig. S25. HPLC trace of a solution of **FFA** (right, 2.209 min) in acetonitrile containing approx. 2 mol% **H_2FFA** (left, 1.311 min).

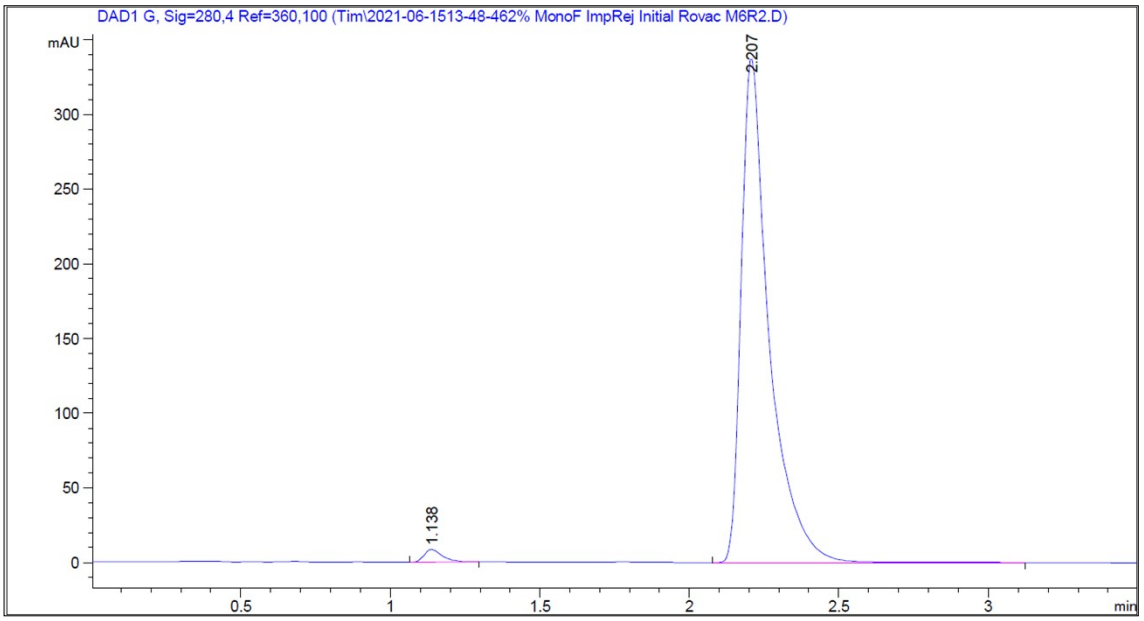


Fig. S26 HPLC trace of a solution of **FFA** (right, 2.207 min) in acetonitrile containing approx. 2 mol% **HF_2FA** (left, 1.138 min).

PXRD

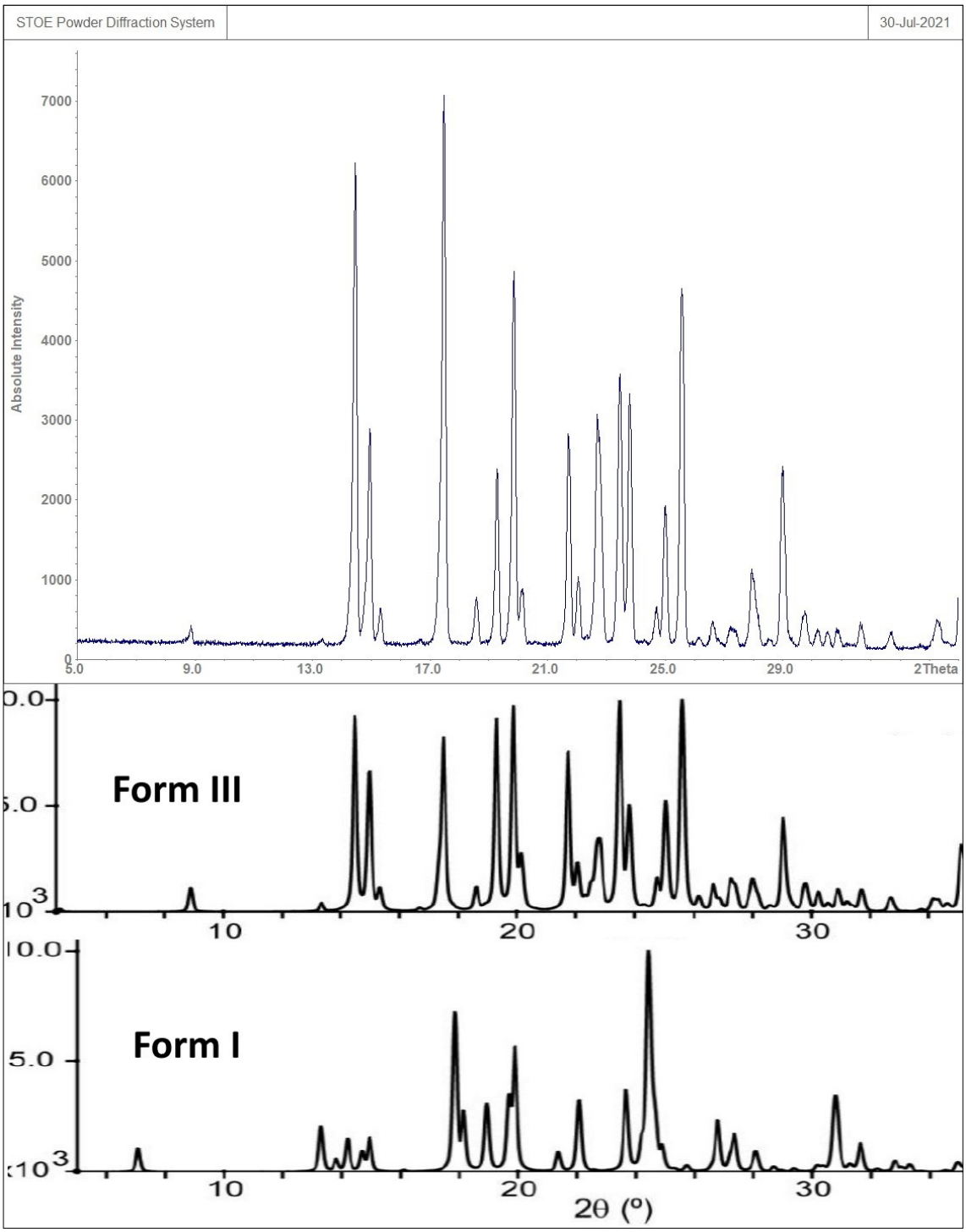


Fig. S27. Measured PXRD pattern of **FFA** recrystallised from EtOH (top) *vs.* literature patterns for Form III and Form I (bottom).[1]

1. V. López-Mejías, J. W. Kampf and A. J. Matzger, *J. Am. Chem. Soc.,* 2012, **134**, 9872-9875.

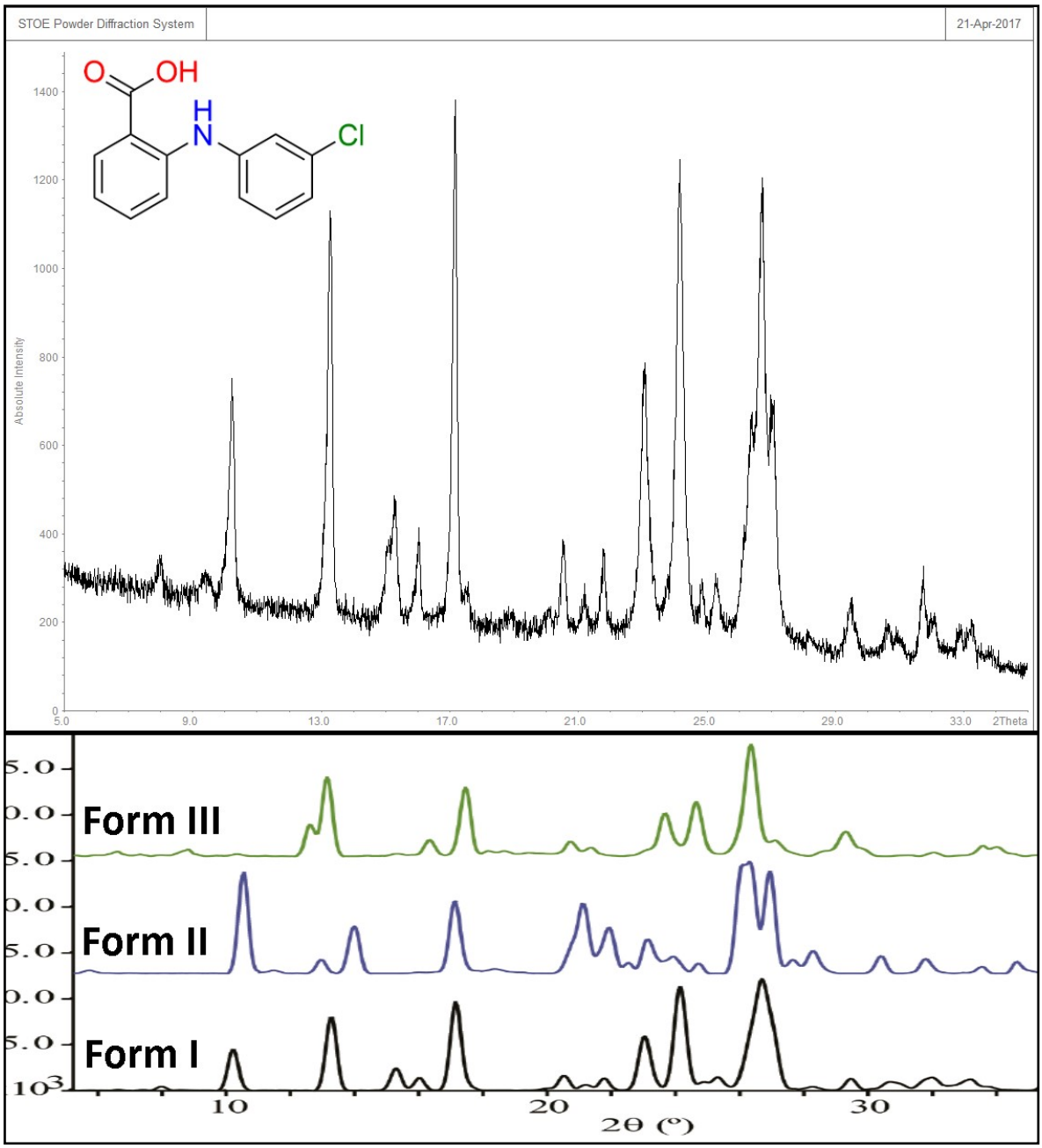


Fig. S28. Top: Measured PXRD pattern of synthesised **ClFA**, bottom: literature patterns of **ClFA** Form I, Form II, and Form III.[2]

2. V. López-Mejías, A. J. Matzger, *Cryst. Growth Des.,* 2015, **15**, 3955–3962.

Crystallisations / Partial Dissolutions



Fig S29. Example of **FFA** crystals grown by the slow evaporation from methanol solution of FFA.

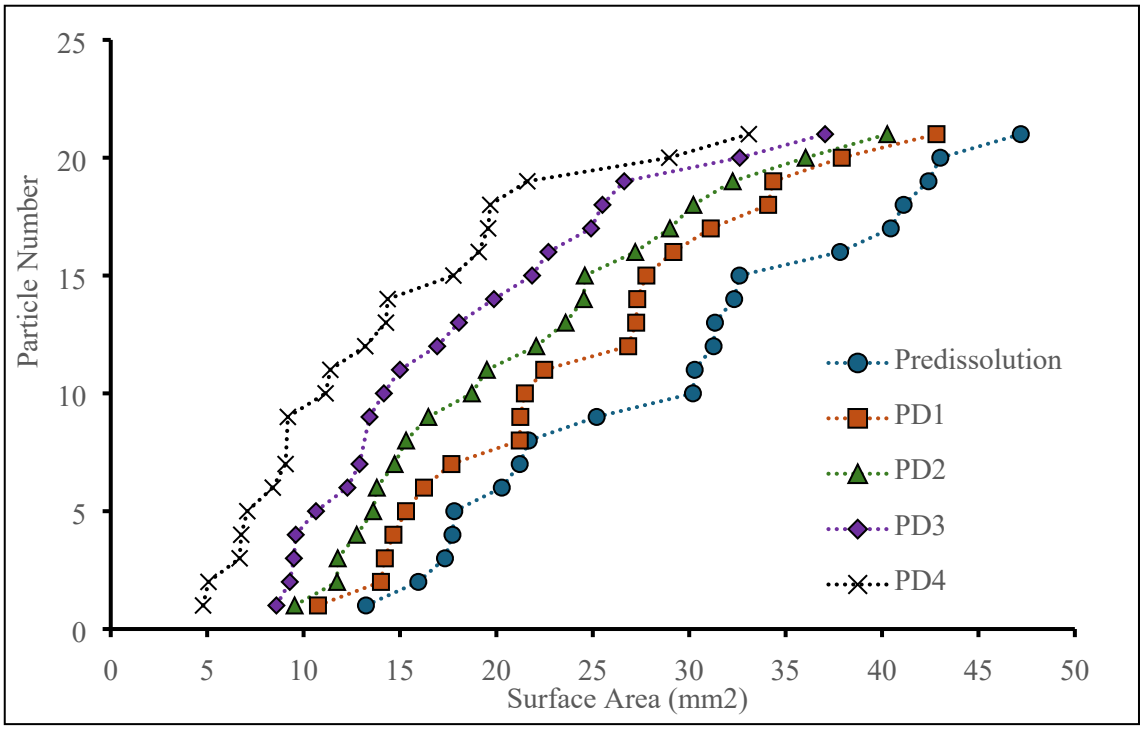


Fig. S30. Surface area distributions for a sample of 20 **FFA** crystals, grown from MeOH solutions containing 2% **HF_2FA**, for the initial sample and for the sample after each of a series of four partial dissolutions.

DSC

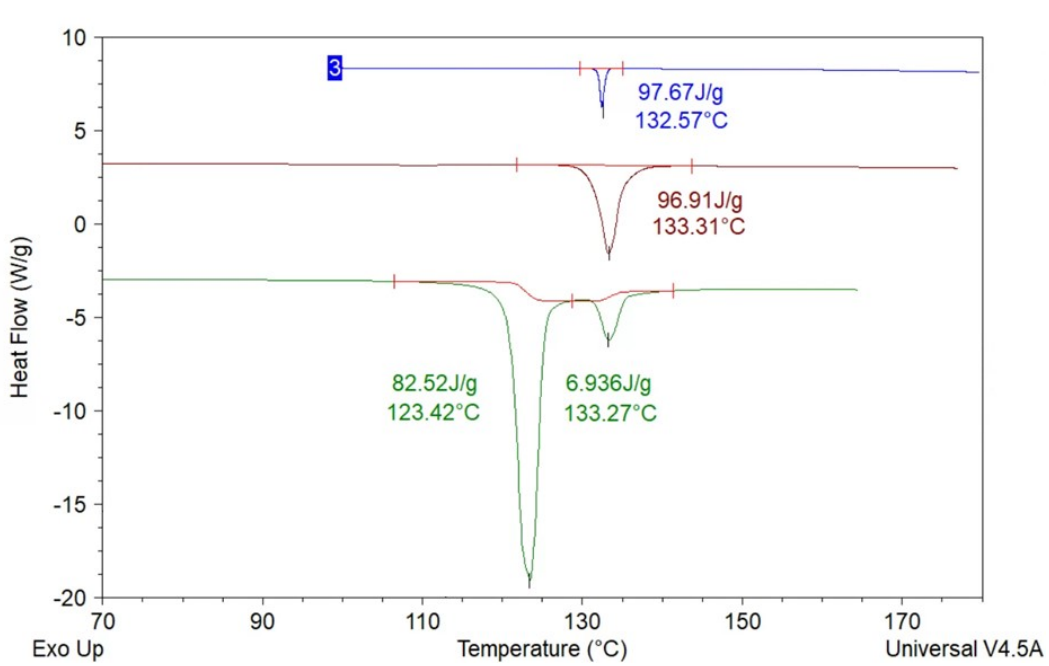


Fig. S31. Top to bottom, DSC curves of **FFA** crystallised with 10 % **ClFA**, collected at heating rates of 1, 10, and 50 °C min^{-1} respectively.

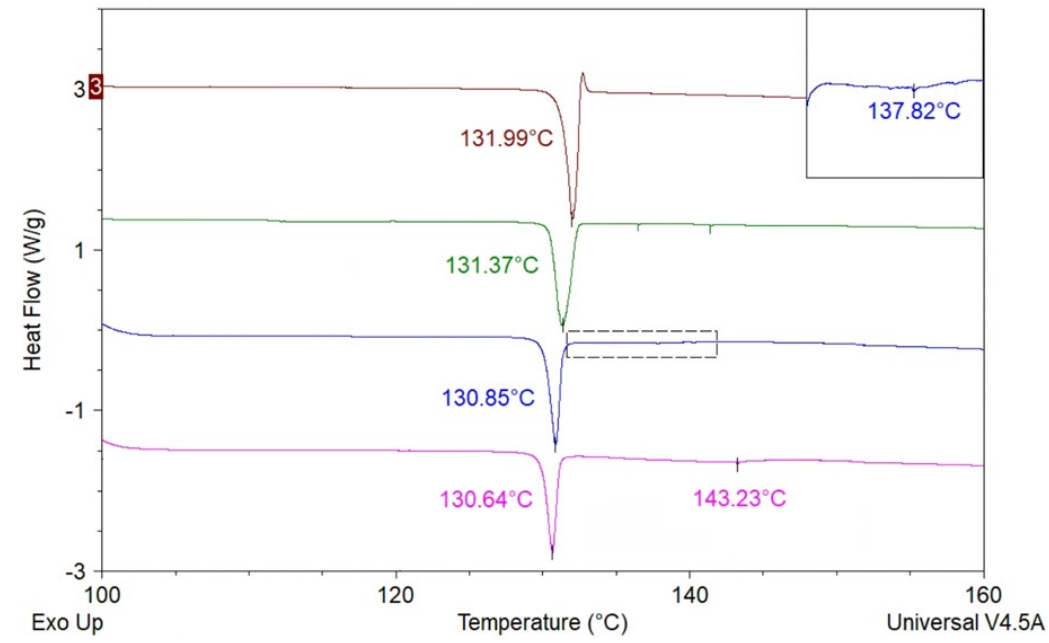


Fig. S32. Top to bottom, DSC curves of **FFA** crystallised with 10%, 20%, 30% and 40% **ClFA**, respectively, collected at a heating rate of 1 min^{-1}. The inset in the top right shows the emergence of the higher melting endotherm.

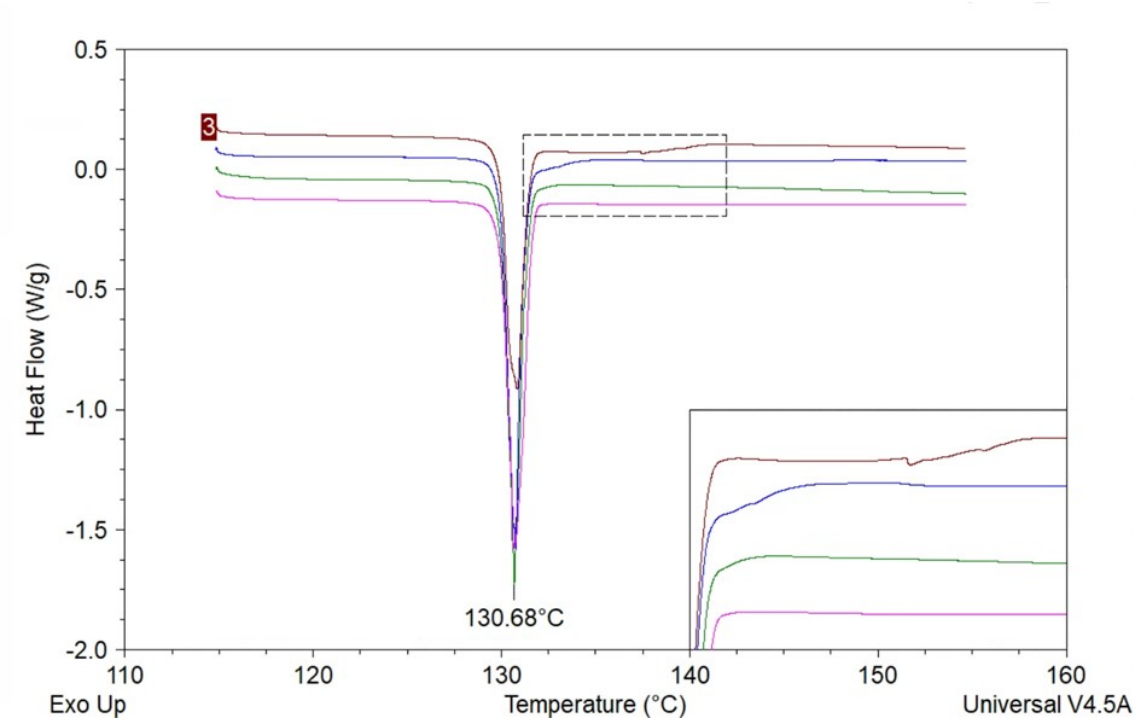


Fig. S33. Bottom to top, DSC curves of **FFA** crystallised with 24%, 26%, 28% and 30% **ClFA**, respectively, collected at a heating rate of 1 °C min^{-1}. The insert on bottom right shows the emergence of the higher melting endotherm.

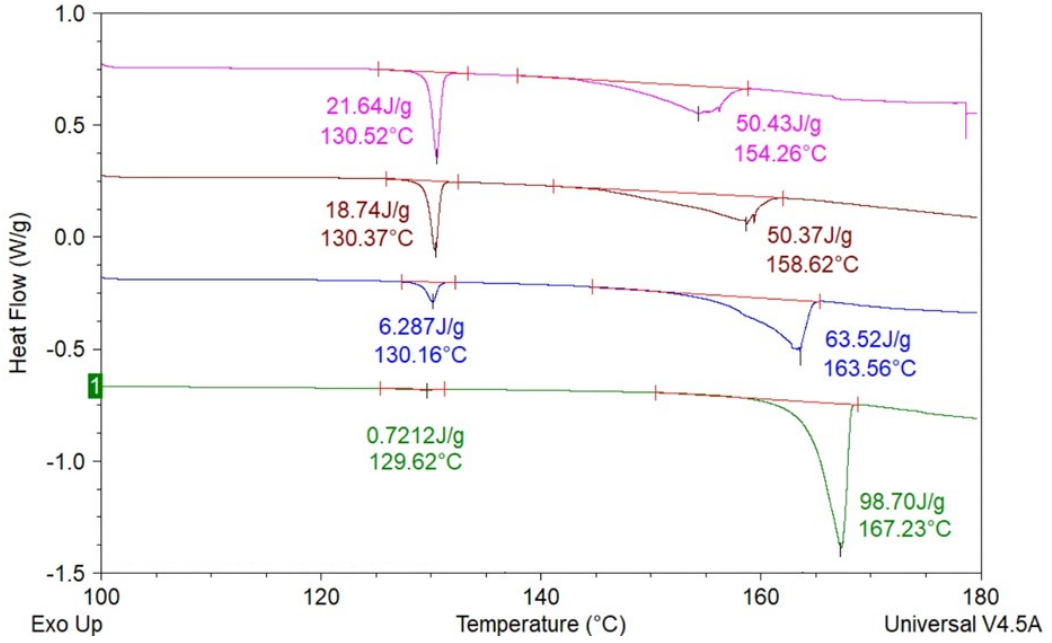


Fig. S34. Top to bottom, DSC curves of **FFA** crystallised with 60%,70%, 80%, 90% **ClFA**, respectively, collected at a heating rate of 1 °C min^{-1}.

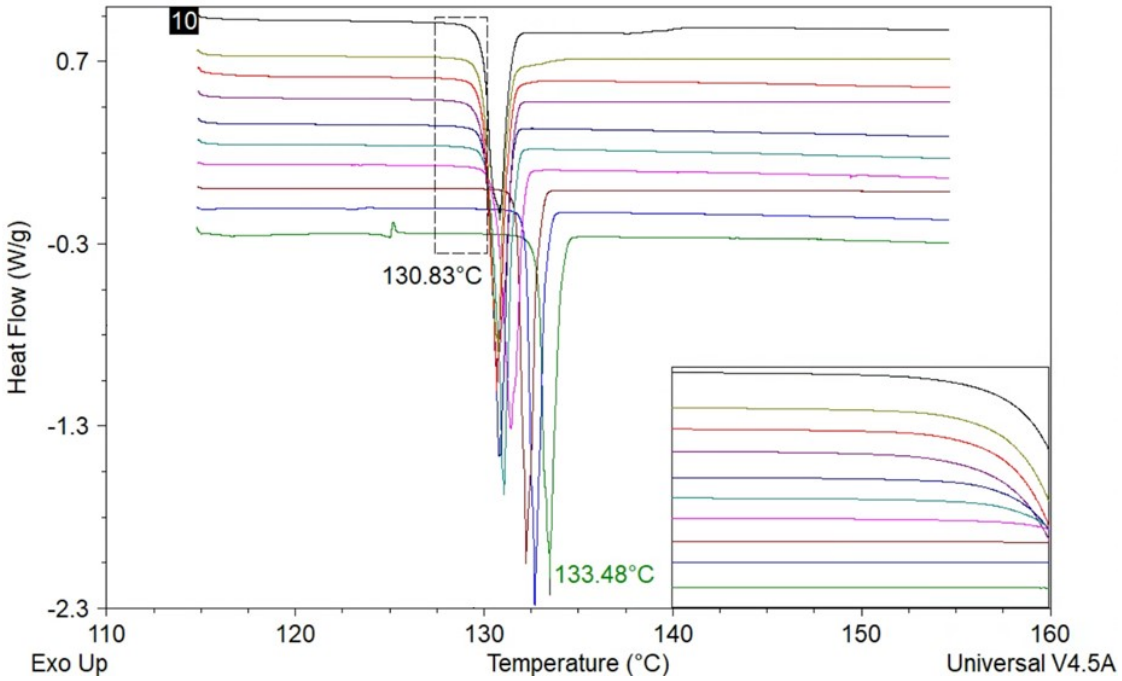


Fig. S35. Bottom to top, DSC curves of **FFA** crystallised with increasing levels of **ClFA**, from 2% to 30%, collected at a heating rates of 1 °C min^{-1}. The insert on the bottom right is an expansion of the region enclosed in dashed lines.

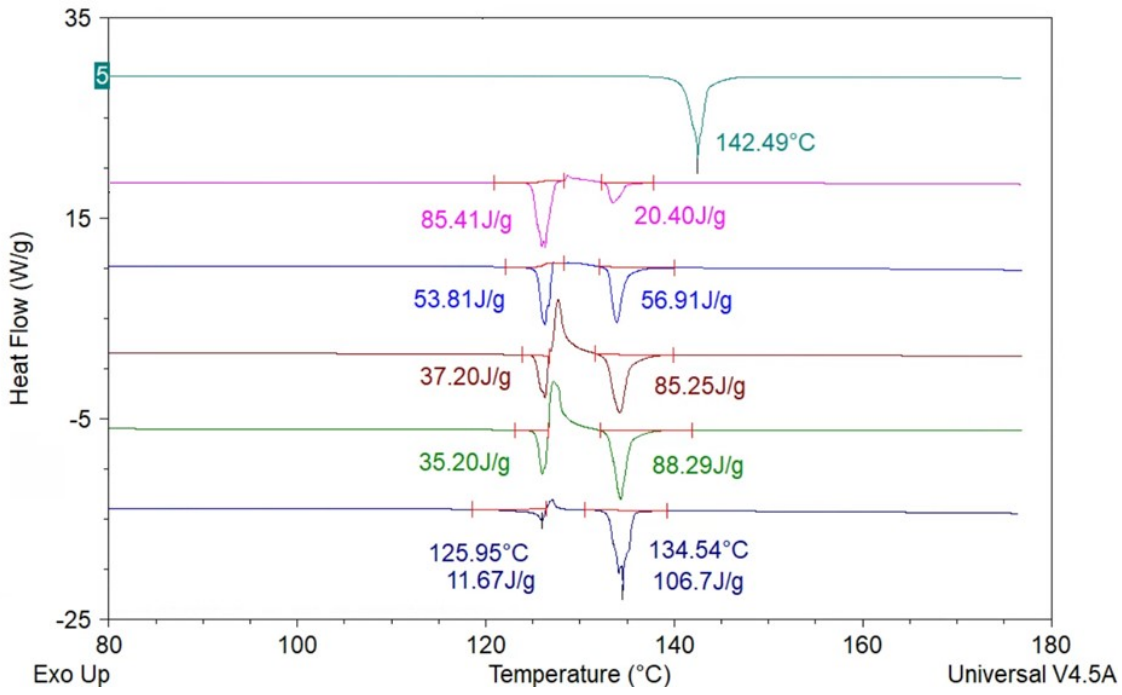


Fig. S36. DSC curves of **FFA** containing, bottom to top 0%, 2%, 3%, 4%, 5% and 100% **HF_2FA**, collected at a heating rate of 10 °C min^{-1}.

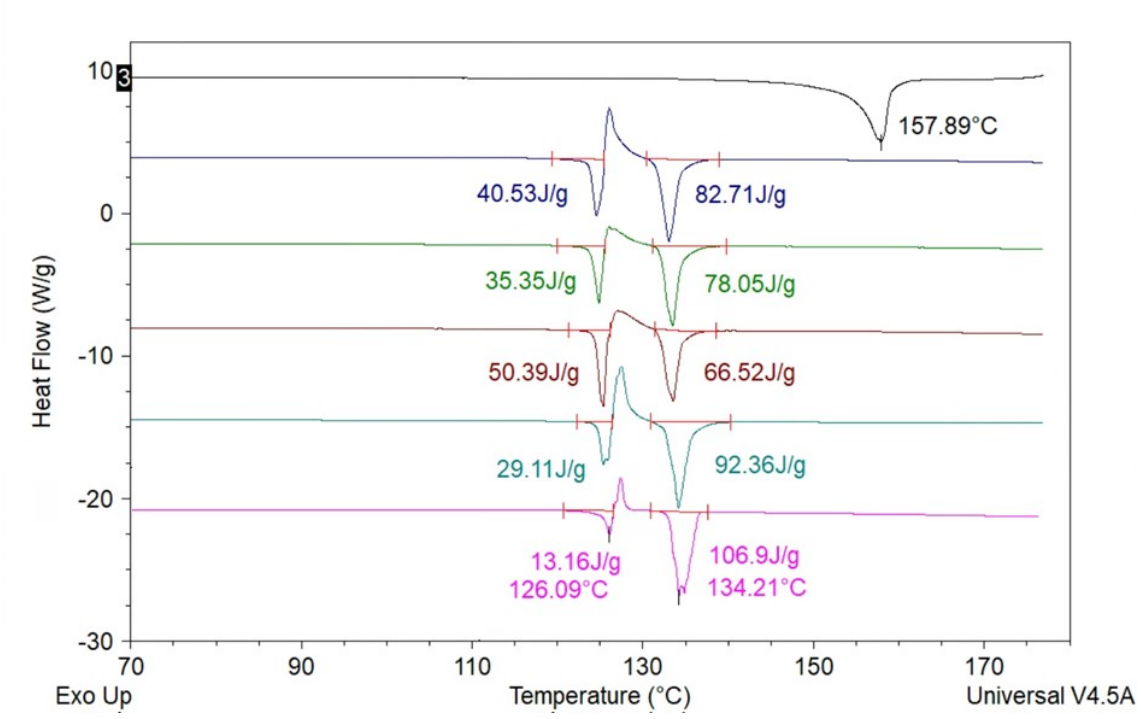


Fig. S37. DSC curves of **FFA** containing, bottom to top, 0%, 2%, 3%, 4%, 5 % and 100% **H_2FFA**, collected at a heating rate of 10 °C min^{-1}.

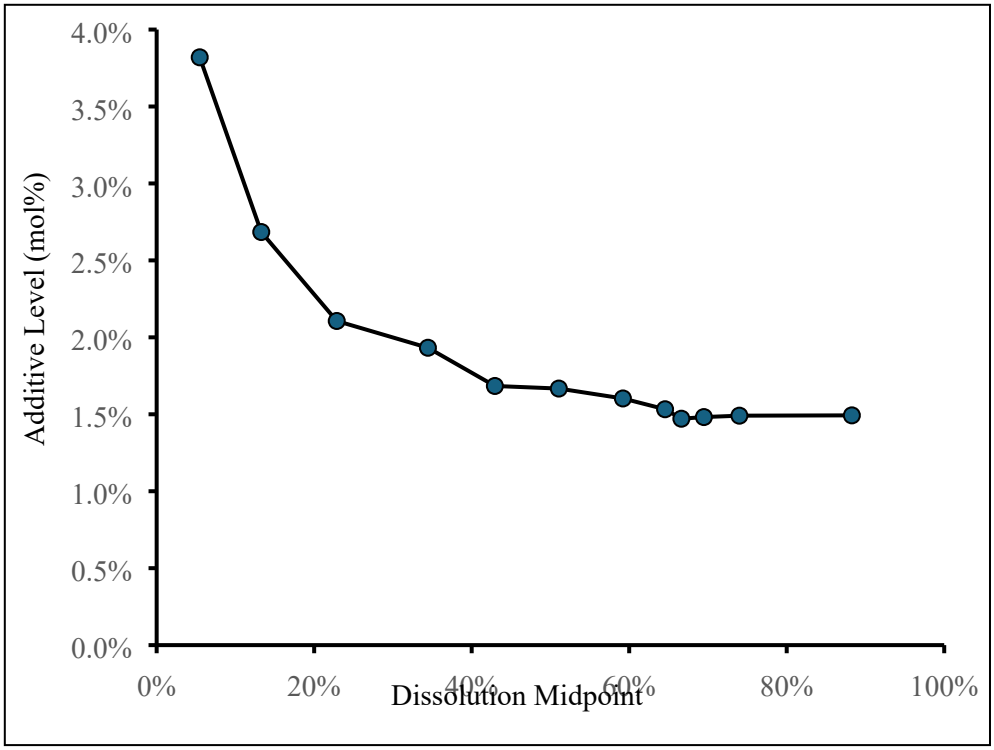


Fig. S38. Plot of **ClFA** level *vs* dissolution midpoint of a sample of 10 crystals of FFA grown from solution containing 2% **ClFA**.

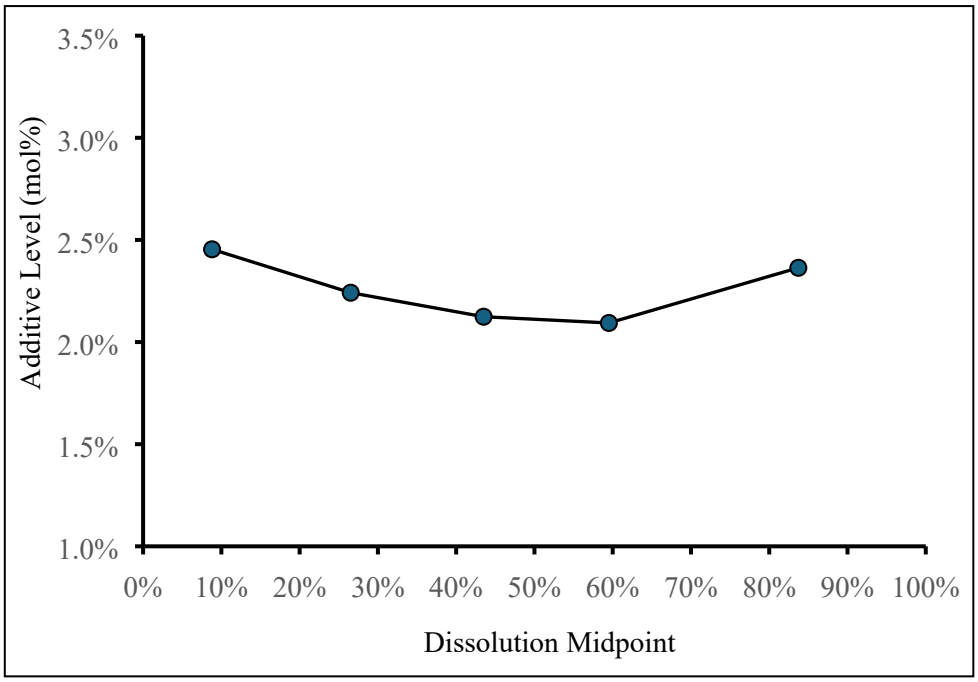


Fig. S39. Plot of **ClFA** level *vs* dissolution midpoint of a large single crystal of **FFA** grown from solution containing 2% **ClFA**.

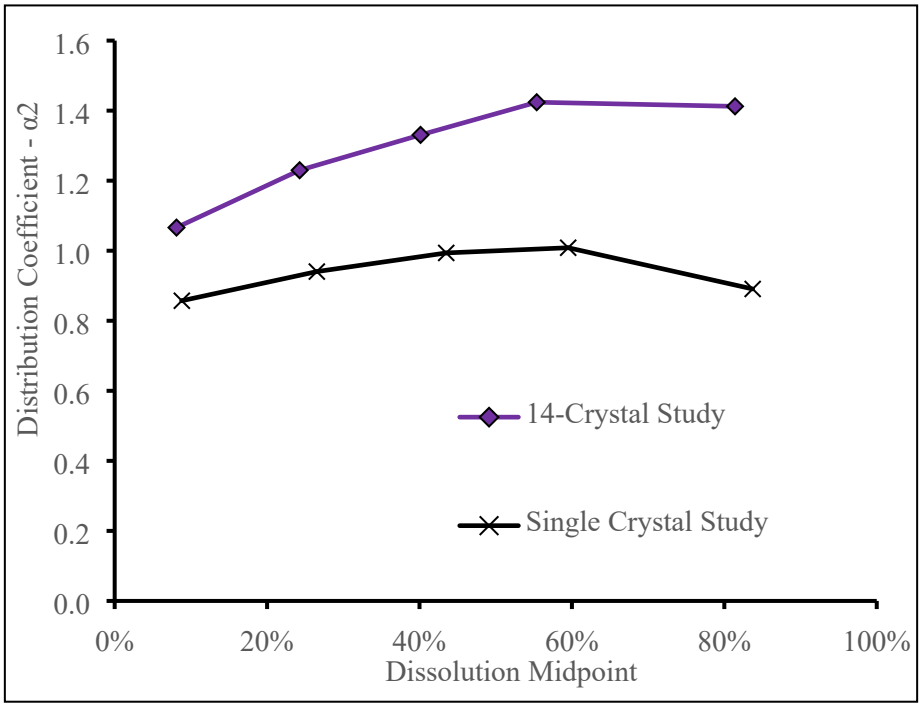


Fig. S40. Plot of α_2 value *vs.* dissolution midpoint a sample of 14 crystals or **FFA**, and also of a large single crystal of **FFA**, grown from solutions containing 2% **ClFA**.

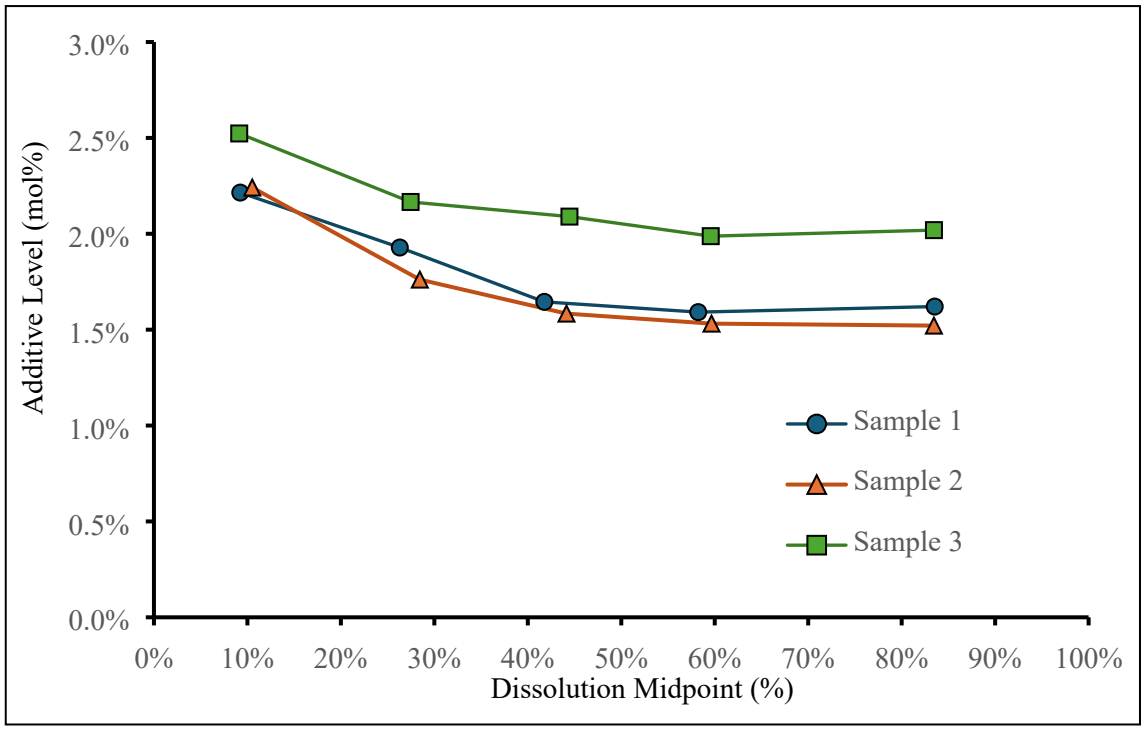


Fig. S41. Plot of **HF_2FA** level *vs* dissolution midpoint of three separate samples of crystals of **FFA** grown from solutions containing 2% **HF_2FA**.